Mon. Not. R. Astron. Soc. **302,** 253–276 (1999)

Modelling of the non-thermal flares in the Galactic microquasar GRS 1915+105

A. M. Atoyan[1,2]⋆ and F. A. Aharonian[1]⋆

[1] *Max-Planck-Institut für Kernphysik, Postfach 103980, D-69029 Heidelberg, Germany*

[2] *Yerevan Physics Institute, Alikhanian Brothers 2, 375036 Yerevan, Armenia*

Accepted 1998 August 18. Received 1998 May 27; in original form 1997 August 29

ABSTRACT

The microquasars recently discovered in our Galaxy offer a unique opportunity for a deep insight into the physical processes in relativistic jets observed in different source populations. We study the temporal and spectral evolution of the radio flares detected from the relativistic ejecta in the microquasar GRS 1915+105, and propose a model that suggests that these flares are caused by synchrotron radiation of relativistic electrons suffering radiative, adiabatic and energy-dependent escape losses in fast-expanding plasmoids (radio clouds). Analytical solutions to the kinetic equation for relativistic electrons in the expanding magnetized clouds are found, and the synchrotron radiation of these electrons is calculated. Detailed comparison of the calculated radio fluxes with the ones detected from the prominent flare of GRS 1915+105 during 1994 March/April provides conclusive information on the basic parameters in the ejecta, such as the absolute values and temporal evolution of the magnetic field, the speed of expansion, the rates of continuous injection of relativistic electrons into and their energy-dependent escape from the clouds, etc. The data from radio monitoring of the pair of resolved ejecta enable unambiguous determination of the parameters of the bulk motion of the counter-ejecta and the degree of asymmetry between them, and also contain important information on the prime energy source for accelerated electrons. These data allow us, in principle, to distinguish between the scenarios of bow-shock powered and relativistic magnetized wind powered plasmoids. Assuming that the electrons in the ejecta can be accelerated up to very high energies, we also calculate the fluxes of the synchrotron and inverse Compton components of the radiation that could be expected during the flares in the broad band from radio frequencies to very high-energy γ-rays.

Key words: radiation mechanisms: non-thermal – stars: individual: GRS 1915+105 – galaxies: jets – gamma-rays: theory – radio continuum: stars.

1 INTRODUCTION

The hard X-ray transient GRS 1915+105, discovered in 1992 (Castro-Tirado et al. 1994), belongs to the class of Galactic black hole (BH) candidate sources characterized by an estimated mass of the compact object $M \geq 3\mathrm{M}_{\odot}$ and strong variability of the electromagnetic radiation, with the spectra extending to energies beyond 100 keV (e.g. see Harmon et al. 1994). The discovery of apparent superluminal jets in GRS 1915+105 (Mirabel & Rodriguez 1994, hereafter MR94), and in another hard X-ray transient, GRO J1655–40 (Tingay et al. 1995; Hjellming & Rupen 1995), provides new convincing evidence that invokes the similarity of these sources with active galactic nuclei (AGNs), the objects powered by the accreting BHs of essentially larger mass-scales. The existence of relativistic jets in these Galactic sources, called 'microquasars', makes them unique cosmic laboratories that allow a deeper insight into the complex phenomenon of the jets common in powerful extragalactic objects (Mirabel & Rodriguez 1995). Indeed, being much closer to us than AGNs, the microquasars offer an opportunity for monitoring the jets over much shorter spatial and temporal scales. Furthermore, the parameter $L_{\rm Edd}/d^2$, where $L_{\rm Edd} = 1.3 \times 10^{38}(M/\mathrm{M}_{\odot})\,\mathrm{erg\,s^{-1}}$ is the Eddington luminosity (an indicator of the potential power of the source) and d is the distance to the source, is typically higher by 2–4 orders of magnitude for the Galactic BH candidates than for AGNs. This enables detection of Galactic superluminal jets with Doppler factors as small as $\delta \leq 1$, in contrast to the case of jets in blazars (AGNs with jets close to the line of sight),

⋆ E-mail: atoyan@fel.mpi-hd.mpg.de (AMA); aharon@fel.mpi-hd.mpg.de (FAA)

which are detected mostly because of their large Doppler factors, $\delta \gg 1$, when strong Doppler boosting of the radiation occurs. Importantly, for the jets with aspect angles close to 90° (which is the case in both GRS 1915+105 and GRO J1655−40), the Doppler factors of the approaching and receding components are not very different, so both components may be detectable (see Mirabel & Rodriguez 1995).

In this paper we present the results of a theoretical study of the non-thermal flares of GRS 1915+105, which are observed in the radio (MR94; Mirabel & Rodriguez 1995; Rodriguez et al. 1995; Foster et al. 1996) and infrared (Sams, Eckart & Sunyaev 1996; Fender et al. 1997; Mirabel et al. 1998; Eikenberry et al. 1998) bands, and can be expected at higher photon energies as well, if the electrons in the ejecta are accelerated up to very high energies (VHE). The main part of the paper is devoted to the explanation of the temporal and spectral behaviour of the prominent 1994 March/April radio flare (MR94). The study of this particular flare is of special interest, because for the first time both components of a superluminal jet source have been clearly resolved, the flare was very strong and the longest (> 40 d) detected so far, and the monitoring of this flare resulted in very important information about the spectral evolution of radio fluxes from the *pair* of ejecta on the conveniently short time-scale of days (to be compared with thousands of years for extragalactic jets). All this may provide experimental information of new quality about the underlying physical processes, making the resolved pairs of microquasar jets very attractive objects for theoretical analyses and modelling.

The model scenario that we propose (Section 2) interpretates the resolved radio sources in GRS 1915+105 as a pair of expanding discrete plasmoids (i.e. clouds containing relativistic electrons and magnetic fields), as is apparently observed, with a continuous supply or in-situ acceleration of radio electrons. Different modifications of the basic approach of expanding radio clouds for the interpretation of variable radio sources have been suggested in a number of earlier works (e.g. Shklovskii 1960; Kardashev 1962; van der Laan 1966; Marscher & Brown 1975). Band & Grindlay (1986) applied this model to interpretation of the non-thermal radiation of SS 433, assuming the propagation of magnetized clouds in subrelativistic ($\beta \approx 0.26$) jets for this source.

In Section 3 we develop the formalism for the detailed study of the evolution of the energy distribution of relativistic electrons in an expanding magnetized medium for an arbitrary time-dependent injection rate, taking into account both adiabatic and radiative energy losses of electrons, as well as losses caused by the escape of electrons in the most general, i.e. *energy*- and *time*-dependent, form. Note that the inclusion of the energy-dependent escape of electrons from the cloud is one of the principal features of our model, which enables us, in particular, to explain the rather fast steepening of the radio spectra observed for GRS 1915+105 during strong flares.

The developed formalism is applied in Section 4 for modelling and comparative analyses of the temporal and spectral evolution of radio fluxes detected from both approaching and receding components of the prominent and most informative flare of GRS 1915+105 in 1994 March/April reported by MR94. Some of the model parameters, like the power-law indexes of the electron injection spectrum ($Q \propto \gamma^{-2}$) or of the escape time ($\tau_{\rm esc} \propto \gamma^{-1}$), can be reliably fixed on the base of simple qualitative arguments. Detailed comparison of numerical calculations with the experimental data allows us to limit rather tightly all other model parameters, like the index $m \simeq 1$ in the dependence of the magnetic field of the cloud on radius ($B \propto R^{-m}$), or the parameters describing the gradual decline of the *continuous* injection rate of electrons and the deceleration of the cloud expansion. Importantly, accurate modelling and comparison of the temporal evolution of the fluxes detected from the approaching and receding radio components of this flare allow us to conclude that these data likely contain important evidence about the prime energy source for continuous energization of the twin ejecta (presumably a continuous flux of energy in the form of a relativistic magnetized wind propagating in the jet region).

After limiting, from the radio data, the basic parameter space characterizing the expanding plasmoids, in Section 5 we speculate that in GRS 1915+105, similarly to the case of BL Lacs (e.g. Urry & Padovani 1995), the electrons may be accelerated beyond the 'radio domain' of GeV energies up to TeV energies, $E \geq 10^{12}$ eV, and we discuss the fluxes of synchrotron radiation, which could then extend beyond the X-ray region, as well as the fluxes of the inverse Compton (IC) γ-rays expected at high and very high energies. The results of the paper are discussed and summarized in Section 6.

2 BASIC ESTIMATES AND MODEL SCENARIO

2.1 Signatures of expanding sources during outbursts

The radio emission of GRS 1915+105 in its active state is characterized by the increase of the radio emission at $\nu \sim 1-10$ GHz from the flux level $S_\nu \leq 10$ mJy to $S_\nu \sim 100$ mJy (the *plateau* state, according to Foster et al. 1996), on top of which the episodes of radio *flares*, with durations from days to a month and fluxes up to ∼1 Jy , are superimposed. The spectra in the plateau state are flat or inverted, $\alpha_{\rm r} \leq 0$ (for $S_\nu \propto \nu^{-\alpha_{\rm r}}$), indicating a significant synchrotron self-absorption in the source. The radio flares, which most probably are related to the events of ejection of radio clouds, are distinguished by a very rapid (less than a day) rise of the fluxes which then decay on time-scales of days or longer. Already at the rising stage of the flares the spectra reveal a transition from optically thick ($\alpha_{\rm r} \leq 0$) to optically thin ($\alpha_{\rm r} > 0$) emission. Remarkably, the gradual transition from self-absorbed to optically thin spectra at progressively lower frequencies is a typical indicator of the synchrotron radiation of an expanding radio cloud (e.g. van der Laan 1966; Pacholczyk 1970).

Convincing examples of such spectral behaviour are given by Rodriguez et al (1995), who summarize the detailed data from radio monitoring of GRS 1915+105 at different wavelengths during five months from 1993 December 1 to 1994 April 30. Thus, the spectrum of the flare on 1993 December 6.0, measured with VLA simultaneously at five different frequencies from 1.47 to 22.49 GHz, was self-absorbed in the range $1.47 \leq \nu \leq 4.89$ GHz ($\alpha_{\rm r} \approx -0.73$), whereas at higher frequencies it corresponded to optically thin synchrotron emission, with mean slope $\alpha_{\rm r} \simeq 0.52$ in the range $4.89 \leq \nu \leq 22.49$ GHz. On that day the flux at $\nu \approx 4.89$ GHz was $S_\nu \approx 500$ mJy . By December 6.6 the fluxes had increased further, reaching $S_\nu = 1083$ mJy at 3.28 GHz and 123 mJy at $\nu = 234$ GHz. Although the latter is the only case of flux measurements

by the IRAM telescope found in table 1 of Rodriguez et al. (1995) at that high frequency, it enables a number of important conclusions. First, it shows that in this broad range the spectrum was 'optically thin', with $\alpha_r = 0.51$, practically the same as on December 6.0, indicating that the source became transparent down to $\simeq$3 GHz frequencies over a time-scale of $\leq$14 h. Secondly, it shows that at least in some of the strong flares the hard spectrum $\alpha_r \simeq 0.5$ may extend in frequency range over 2 orders of magnitude. Thirdly, extrapolating the December 6.6 flux from 3.28 GHz with $\alpha_r \simeq 0.5$, we can conclude that, indeed, the flux at 4.89 GHz, which already corresponded to 'optically thin' emission on December 6.0, should have been increased by a factor of $\sim$2, reaching $\simeq$900 mJy. This would require *continuous* and significant injection of freshly accelerated electrons into the radio source, since otherwise the expansion of the source would result only in a strong decrease of the fluxes at optically transparent frequencies.

Remarkably, the clear signatures of expanding radio clouds are found not only for the strong flares reaching the 1-Jy level, but also in the more frequent flares of smaller scales, as recently reported by Mirabel et al. (1998) for the $\leq$100 mJy flare of 1997 May 15, which over a time-scale of $\leq$1 hr became transparent at progressively longer wavelengths from 2.2 μm to 6 cm.

It should be noted, with respect to the possibility of modelling the radio flares in GRS 1915+105 in terms of relativistically moving and expanding radio clouds, that observations of the 1994 March/April flare have revealed an interesting feature which could be interpreted as contradicting the cloud model in principle. Namely, the detection of both approaching and receding ejecta of this flare has resulted in the relevant flux ratio $S_a/S_r = 8 \pm 1$ measured at equal angular separations of the ejecta from the core (MR94). For the deduced values of relativistic speeds of the ejecta, $\beta \simeq 0.92$ moving in opposite directions at the angle $\theta = 70°$ (resulting in apparent superluminal motion with $\simeq 1.25c$ at distance $d = 12.5 \pm 1.5$ kpc, see MR94), this ratio is significantly smaller than $S_a/S_r \simeq 12$, which was expected for the fluxes produced in the case of real motion of *discrete* radio clouds, as was apparently observed. This feature can be interpreted as an indication of shocks propagating with the speed $\beta \simeq 0.92$ in the continuous fluid of radio-emitting plasma that is streaming with a velocity $\beta_f \simeq 0.7$ (Bodo & Ghisellini 1995). However, it is possible to explain the observed flux ratio in terms of the real motion of discrete radio sources with speeds coinciding with the deduced pattern speed, if one allows for the twin ejecta being *similar*, but not necessarily identical, as was actually implied in previous calculations of the ratio $S_a/S_r \simeq 12$. In Section 4 we will show that the discrepancy between the observed and 'expected' flux ratios is easily removed by a small asymmetry between the ejecta, e.g. by a small difference in the velocities β_a and β_r of the approaching and receding clouds. Then, deviations of S_a/S_r from the 'expected' value can be considered as a measure of asymmetry between the twin ejecta. Detailed discussion of this subject is given elsewhere (Atoyan & Aharonian 1997).

2.2 Magnetic fields, size and speed of expansion of radio clouds

Power-law radiation spectra with $\alpha_r \simeq 0.5$ imply a power-law distribution of relativistic electrons $N(\gamma) \propto \gamma^{-\alpha_e}$ with $\alpha_e = 2\,\alpha_r + 1 \simeq 2$. As these radio spectra may span a broad interval of frequencies from $\sim$1 GHz to $\leq$250 GHz, the electron distribution should be a power law within some interval of energies $\gamma_1 \leq \gamma \leq \gamma_2$, with the ratio of Lorentz factors $\gamma_2/\gamma_1 > 10$. To estimate the range of basic parameters of radio clouds, such as the magnetic field B, size R, speed of expansion v_{exp}, etc., in this section we will suppose an electron distribution $N(\gamma) = A_0\gamma^{-2}$ extending from $\gamma_1 = 1$ up to $\gamma_2 = \gamma_{max}$, with a sharp cut-off above γ_{max}, i.e. $N(\gamma > \gamma_{max}) = 0$.

The characteristic frequency of synchrotron photons emitted by an electron with Lorentz factor γ in the magnetic field B is $\nu_s \simeq 0.3 \times (1.5\nu_B\,\gamma^2)$, where $\nu_B = eB \sin\vartheta/2\pi m_e c$, and ϑ is the pitch angle (e.g. Ginzburg 1979). For the mean $\overline{\sin\vartheta} = \sqrt{2/3}$, the frequency is

$$\nu_s \simeq 10^6\, B\gamma^2 \text{ Hz}, \tag{1}$$

where B is in Gauss. As the magnetic fields expected in the cloud on time-scales of few days after ejection are $B \sim 0.03{-}0.3$ G (see below), for the production of synchrotron photons at $\nu \sim 300$ GHz electrons with $\gamma\sim$ a few times 10^3 are required. Similar electron energies must be reached even in the case of significantly less powerful flares to provide the synchrotron emission observed in the K band ($\lambda \approx 2.2$ μm) on time-scales of hours, when $B \sim 10$ G (Fender et al. 1997; Mirabel et al. 1998). Meanwhile, the synchrotron origin of the infrared jet observed by Sams et al. (1996) would imply relativistic electrons with $\gamma \gg 10^4$. However, in the first part of this paper, where we study the radio fluxes, we will limit the range of relativistic electrons under consideration to those with $\gamma_{max} = 10^4$.

In the case of an isotropic source with spectral luminosity $L'(\nu')$ in its rest frame, an observer at a distance d would detect the flux $S_\nu = \delta^3 L'(\nu/\delta)/4\pi d^2$, where $\delta = \sqrt{1-\beta^2}/(1-\beta\cos\theta)$ is the Doppler factor of the source moving with a speed β at an angle θ to the line of sight (e.g. Lind & Blandford 1985). For distances $d_* \equiv d/12.5$ kpc $\simeq 1$, the fluxes expected from an optically thin cloud are

$$S_\nu \simeq 2 \times 10^{-39}\, A_0\, \delta^{7/2}\, B^{3/2}\, \nu^{-1/2}\, d_*^{-2} \text{ mJy}. \tag{2}$$

Introducing the ratio $\eta = w_e/w_B$ of the energy densities of relativistic electrons $w_e = 3W_e/4\pi R^3$ to the energy density of the magnetic field $w_B = B^2/8\pi$ in the cloud, the coefficient A_0, which corresponds to the total number of electrons, can be expressed as $A_0 = 2 \times 10^{50}\,\eta\, B^2 R_{15}^3$, where R_{15} is the characteristic radius R of the cloud in units of 10^{15} cm. As, for strong flares, the radio fluxes observed at $\nu \sim 10$ GHz reach the level $\sim$500 mJy, for the normalized flux $S_* \equiv S_{10\,GHz}/500$ mJy ~ 1 the magnetic field should be

$$B = 7.7 \times 10^{-2}\, \delta^{-1}\, \eta^{-2/7} R_{15}^{-6/7} d_*^{4/7} S_*^{2/7} \text{ G}. \tag{3}$$

The radius R of the cloud can be estimated from the requirement of optical transparency of the source with respect to synchrotron self-absorption. Calculation of the absorption coefficient (e.g. Ginzburg 1979) results in $\kappa_\nu = 4.4 \times 10^{15} \eta B^4 \nu^{-3}$ cm^{-1}. Using equation (3), the

radius R can be expressed in terms of the opacity $\tau_\nu = R\,\kappa_\nu$ at a given frequency ν:

$$R_{15} = 0.46\,\delta^{-28/17}\eta^{-1/17}d_*^{16/17}S_*^{8/17}\tau_\nu^{-7/17}\nu_{\rm GHz}^{-21/17}\ , \tag{4}$$

where $\nu_{\rm GHz} \equiv \nu/1$ GHz. Then from equation (3) it follows that

$$B = 0.15\,\delta^{7/17}\eta^{-4/17}d_*^{-4/17}S_*^{-2/17}\tau_\nu^{6/17}\nu_{\rm GHz}^{18/17}\ {\rm G}. \tag{5}$$

For the ejecta in GRS 1915+105 the Doppler factor $\delta \simeq 0.6$ (MR94), so the optical transparency $\tau_\nu \leq 1$ at frequencies $\nu \sim 1.4{-}3$ GHz requires a magnetic field at the stage of flare maximum $B \sim 0.2{-}0.3$ G, if the energy densities of relativistic electrons and magnetic fields in the ejecta are at the equipartition level $\eta \sim 1$.

Owing to the rather weak dependence of B on the opacity τ_ν, the equipartition magnetic field $B_{\rm eq}$ can be significantly less than 0.2 G only if $\tau_\nu \leq 0.1$. However, to reach even $\tau_\nu = 1$ in a few days after ejection, the clouds should *expand* with a very high speed comparable to the speed of light. Indeed, from equation (4) it follows that the characteristic size of the clouds ejected on 1994 March 19.8, should increase to $R \simeq 8\times10^{14}\tau_{1.4\,\rm GHz}^{-0.41}$ cm by March 24.3, $\Delta t \simeq 4.5$ d after the ejection event, when the flare was detected by the Nancay telescope (Rodriguez et al. 1995). Then, because the intrinsic time in the rest frame of the cloud $\Delta t' = \delta\,\Delta t$, a speed of expansion $v_{\rm exp} > 0.1c$ is required to provide $\tau_{1.4\,\rm GHz} \leq 1$. Expansion speeds even higher are required for the flares that are weaker, but become transparent within $\Delta t \leq 1$ d, like the one reported by Gerard (1996). Thus, the transition of the flares from optically thick to optically thin spectral forms on time-scales of days implies that the radio clouds are expanding with velocities $v_{\rm exp} \geq (0.1{-}0.2)c$. This estimate agrees with the expansion speed of the clouds deduced from the observations, and suggests that the lack of redshifted optical lines from GRS 1915+105 might be a result of their large Doppler broadening (Mirabel et al. 1997).

2.3 Steepening of the radio spectra: implications

A very significant feature of the spectral evolution of the radio flares in GRS 1915+105 is that initially hard spectra, typically with $\alpha_{\rm r} \sim 0.5$ when the fluxes are at the maximum level, later on steepen to $\alpha_{\rm r} \sim 1$ when the flares are fading out. Thus, from table 1 of Rodriguez et al. (1995) one can see that the fluxes of the strong outburst of 1993 December 11, measured by Nancay telescope at 21 and 9 cm, corresponded to $\alpha_{\rm r} \simeq 0.45$. On the next day the fluxes had decreased by a factor of 2, while the spectrum steepened to $\alpha_{\rm r} \simeq 0.6$. Gradual steepening of the radio spectra in time is apparent also in the multiwavelength VLA data taken on December 14, 16 and 17, when the spectral slope between 4.89 and 22.49 GHz was changing as $\alpha_{\rm r} \simeq 0.72$, 0.83 and 1.1, respectively.

Perhaps the most valuable example of gradual steepening of the radio spectra during the evolution of the flare in time is provided by the prominent outburst of 1994 March 19, when the pair of relativistic radio clouds has been resolved. On March 24 the spectral index between $\lambda = 2$ and 6 cm was $\alpha_{\rm r} = 0.5 \pm 0.1$, which by April 16 steepened to $\alpha_{\rm r} = 0.84 \pm 0.03$ (MR94). Importantly, on April 16 the spectra of both components, well resolved by that time, corresponded to the same spectral index (within the quoted uncertainties), confirming the expected similarity of the counter-jets, and therefore allowing one to consider with more confidence the spectral evolution observed for the *total* flux (which only is available for the flares remaining unresolved) as a characteristic feature of each cloud of the ejected pair.

The steepening of the radio spectra from initial $\alpha_{\rm r} \simeq 0.5$ to $\alpha_{\rm r} \simeq 1$ requires a steepening of the electron energy distribution from the power-law index $\alpha_{\rm e} \simeq 2$ to $\alpha_{\rm e} \simeq 3$. Modification of the energy distribution of electrons by a factor of 1 ('power-law break') could be attributed to the radiative (synchrotron and/or IC) energy losses $P_{\rm s}(\gamma) \propto \gamma^2$ for electrons continuously injected into the emission region, and for extragalactic jets models of this kind have been considered in a number of papers (e.g. Marscher 1980; Königl 1981; Bloom & Marscher 1996). In the case of GRS 1915+105, however, such an interpretation of the radio data is problematic.

Indeed, the synchrotron energy-loss time of an electron with energy γ is

$$t_{\rm s}(\gamma) \simeq 7.7\times10^8\,\gamma^{-1}B^{-2}\ {\rm s}. \tag{6}$$

The break energy in the distribution of electrons formed at a time t is found from the condition $t_{\rm s}(\gamma_{\rm br}) = t$. Then assuming that the evolution of the magnetic field in time behaves as $B = B_0(R_0/R)^m \rightarrow B_0(t_0/t)^m$ (for expansion with a constant speed), and substituting $\gamma_{\rm br}$ into equation (2), the characteristic break frequency of the synchrotron radiation spectrum can be estimated:

$$\nu_{\rm br} \simeq 4\times10^{12}\,(t_0/4.5\ {\rm d})^{-2}B_0^{-3}(t/t_0)^{3m-2}\ {\rm Hz}\ . \tag{7}$$

Thus, for $B_0 \sim 0.2{-}0.3$ G at time $t_0 = 4.5$ d after ejection, given by equation (5), the synchrotron break frequency is orders of magnitude beyond the region $\nu \sim 1{-}10$ GHz. Moreover, the break frequency is increasing with time (unless $m \leq 2/3$ were supposed, which is unreasonably low; see Section 2.5), and therefore this scenario might explain the hardening, but not the steepening, of the radio spectra in time.

One might suppose, nevertheless, that the radiative losses could be responsible for the steepening effect in the scenario, when the injection of radio electrons into the clouds occurs only at earlier stages of the flare, at times $t_* \leq 1$ d, so that the radiative losses would form a break in the electron distribution at some γ_*, which then moves to lower energies as $\gamma_{\rm br}(t) = \gamma_*\,t_*/t$ owing to adiabatic losses, resulting in steepened radio spectra with $\alpha_{\rm r} \simeq 1$ a few days after ejection.

To check this possibility, we have calculated numerically the temporal evolution of the electron distribution in an expanding cloud, assuming an injection spectrum of electrons with $\alpha_{\rm e} = 2$, and injection rate $Q(t) =$ constant for $t \leq t_* = 1$ d and $Q(t) = 0$ for $t > t_*$. The resulting electron distributions in the cloud at different times are shown in Fig. 1. Remarkably, almost immediately (at $\Delta t \sim 0.1t_*$) after the injection of fresh high energy particles ceases, the power-law *break* at the energy γ_* is transformed into a sharp *cut-off* above that energy. This

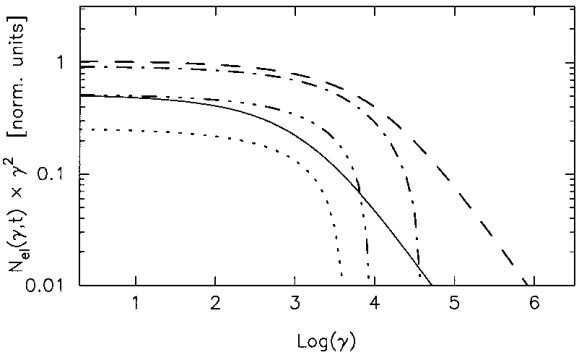

Figure 1. The temporal evolution of the energy distribution of electrons $N(\gamma, t)$ in an adiabatically expanding magnetized cloud calculated in the case of injection of electrons with a constant rate $Q(\gamma, t) = Q_0\gamma^{-2}$ for $t \le t_* = 1$ d and $Q(t) = 0$ for $t > t_*$ (with γ extending to very high energies), assuming that the cloud expands with a constant speed and the magnetic field of the cloud is $B = B_*(t/2\,t_*)^{-2}$ with $B_* = 0.5$ G. The curves plotted with solid, dashed, dot–dashed, 3-dot–dashed and dotted lines correspond to the apparent times $t = 0.5$, 1.0, 1.1, 2 and 4 d. All curves are normalized to the value of $N(\gamma, t)$ at $t = 1$ d and $\gamma = 10$.

may be a rather unexpected result (e.g. if compared with the relevant discussion in Kardashev 1962) but it has a clear explanation: since the energy-loss time t_s of electrons with energies $\gamma > \gamma_*$ is less than t_*, in the absence of freshly injected particles with these energies all the old ones are quickly cooled down to $\gamma \simeq \gamma_*$ by continuous synchrotron losses, even if one assumes the decline of the magnetic fields in the expanding cloud to be as fast as $B \propto R^{-2}$. The power-law break in the spectrum can be maintained only assuming continuous replenishment of high-energy electrons, but then we come back to the estimate of the break frequency given by equation (7).

Modifying the 'adiabatic shift' scenario, one might then suppose that the steepening of the radio spectra could be connected with the *cut-off* energy moving down the energy axis, or, even more generally, assuming that the injection spectrum of electrons is some gradually steepening function, so that the distribution $N(\gamma, t)$ formed at time $t \simeq t_*$ may be a steepening function, not necessarily connected with the radiative cut-off. Perhaps for some particular flares declining extremely fast this modification could work. However, it cannot provide a general explanation for the spectral steepening effect, and in particular it fails for the 1994 March/April flare. Indeed, in the case of negligible injection of new particles, the energy distribution of radio electrons suffering adiabatic losses in the expanding cloud is $N(\gamma, t) = (t/t_*)\,N_0(\gamma t/t_*)$ (Kardashev 1962). For $N(\gamma) \propto \gamma^{-\alpha_e}$ one has $S_\nu \propto B^{(\alpha_e+1)/2} \times N(t)$ (e.g. Ginzburg 1979). Then, even in the case of very slow decline of the magnetic field with $m = 1$ ($m = 2$ seems more appropriate for adiabatically expanding clouds without injection of new particles, see e.g. van der Laan 1966), one readily finds that $S_\nu \propto t^{-2.5}$ at the stages when the radio index $\alpha_r = (\alpha_e - 1)/2 = 0.5$, and $S_\nu(t) \rightarrow t^{-4}$ when $\alpha_r \rightarrow 1$. Meanwhile, the observations reveal a much slower decline rate of the 1994 March/April flare, $S_\nu(t) \propto t^{-1.3}$ (MR94). Importantly, this qualitative estimate shows that for self-consistent interpretation of both the steepening of the radio spectra and the relatively slow rate of decline of the fluxes, as observed, in particular, for the 1994 March/April flare of GRS 1915+105, one has to assume essentially *continuous* injection of radio electrons into the clouds.

We see two principal possibilities to account for the steepening of the radio spectra at the fading stage of the flares. The first one is to assume that the relativistic electrons are continuously injected into the cloud with a spectrum $Q(\gamma, t) \propto \gamma^{-\alpha_{inj}}$, with the power-law index $\alpha_{inj} = 2$ during the first 1−3 d, which later on steepens to $\alpha_{inj} \ge 3$ so as to provide the steepening of the resulting $N(\gamma, t)$ to the power-law index $\alpha_e \sim 3$. The second option is to assume *energy-dependent escape* of electrons from the clouds, while the injection spectrum would not necessarily steepen.

In principle, neither of those two options can be excluded without specification of $Q(\gamma, t)$ and detailed calculations of $N(\gamma, t)$ and $S_\nu(t)$. However, there are some arguments favouring the importance of the escape of relativistic electrons. Indeed, let us suppose that the electron escape is negligible. Then, in order to modify the electron distribution from the power-law index $\alpha_e \sim 2$ at $t_1 \simeq 1$−3 d to $\alpha_e \rightarrow 3$ at $t \sim 2$−3 t_1 (as often observed), the injection of electrons with the steep spectrum $\alpha_{inj} \ge 3$ should proceed *at least* with the same rate $Q(\gamma, t)$ as initially. However, contrary to this requirement, strong steepening of the injection spectrum generally indicates that the efficiency of particle acceleration is essentially dropped, therefore significant decline of the injection rate $Q(\gamma, t)$ should be expected. Meanwhile, allowing fast escape of relativistic electrons from the cloud, the old 'hard spectrum' electrons could be replaced with freshly injected 'soft' ones on time-scales $\tau_{esc} \ll t$; therefore the resulting distribution $N(\gamma, t) \simeq Q(\gamma, t)\,\tau_{esc}$ could respond promptly to variations in the injection spectrum. Moreover, in the case of energy-dependent escape $\tau_{esc}(\gamma) \propto \gamma^{-1}$, the required steepening of $N(\gamma, t)$ may be reached even for the same hard injection spectrum $Q \propto \gamma^{-2}$ as initially.

2.4 Energetics

The energy W_B of the magnetic field in the radio cloud can be estimated using equation (3):

$$W_B \simeq 9.9 \times 10^{41}\,\delta^{-2}\eta^{-4/7}R_{15}^{9/7}d_*^{8/7}S_*^{4/7}\ \text{erg}\,. \tag{8}$$

The total energy $W_{tot} = W_e + W_B \propto (\eta^{3/7} + \eta^{-4/7})$ reaches its minimum at $\eta = 4/3$, i.e. around equipartition between magnetic field and relativistic electrons, as expected (e.g. Pacholczyk 1970). For the ejecta in GRS 1915+105 with $\delta \simeq 0.6$, the energy in radio electrons at the

stage of the flare maximum is estimated, in the case of $\eta \sim 1$, as $W_e \sim 3 \times 10^{42}$ erg, which requires continuous injection of electrons with the mean power $P_{inj} \simeq 1-3 \times 10^{37}$ erg s^{-1} for $\Delta t' \sim 1-3$ d. However, this estimate does not take into account the adiabatic energy losses of electrons, which increase P_{inj} to the level of 10^{38} erg s^{-1} (see Section 4).

If the field B in the cloud deviates from its equipartition value, the energy requirements are significantly higher. Defining B_{eq} as a magnetic field in the case of $\eta = 1$, from equation (5) we find that $\eta = (B/B_{eq})^{-17/4}$. It means that to provide the same flux S_ν, a decrease of B by an order of magnitude is to be compensated by an increase of η by 4 orders of magnitude, resulting in the increase of $W_e \propto \eta^{3/7}$ by almost 2 orders of magnitude. Then, assuming a magnetic field $B_0 \simeq 0.03$ G instead of $B_{eq} \simeq 0.2-0.3$ G, one also has to suppose $P_{inj} \sim 10^{40}$ erg s^{-1}, which significantly exceeds the maximum luminosity of GRS 1915+105 observed in X-rays (Greiner, Morgan & Remillard 1996; Harmon et al. 1997). Thus, $B_0 \geq 0.03$ G should be considered as a rather conservative lower limit for the characteristic magnetic field in the radio clouds at times when the cloud radius $R \simeq 10^{15}$ cm.

Increasing magnetic fields by an order of magnitude beyond equipartition field B_{eq}, would decrease P_{inj} down to 10^{36} erg s^{-1}. However, now the energy in the magnetic field would be strongly increased, therefore in order to account for these magnetic fields we would have to suppose a total power in the jet $P_{jet} \geq 10^{40}$ erg s^{-1}. Moreover, for the fields exceeding B_{eq} even by a factor of 2, the magnetic pressure in the cloud would significantly exceed the pressure of relativistic electrons. In that case one would have to explain why a strongly magnetized cloud is expanding with sub-relativistic speeds (in the opposite case of $\eta \ll 1$ the answer is obvious).

For the estimated energy $W_e \simeq 3 \times 10^{42} \eta^{3/7}$ erg, the total number of relativistic electrons in the cloud is $N_e \simeq 4 \times 10^{47} \eta^{3/7}$. Assumption of an equal amount of protons results in the cloud mass $M_{cl} \simeq 7 \times 10^{23} \eta^{3/7}$ g. The kinetic energy of a cloud moving with the bulk Lorentz factor $\Gamma \simeq 2.5$ is then estimated as $W_{kin} = (\Gamma - 1) M_{cl} c^2 \simeq 10^{45} \eta^{3/7}$ erg, i.e. essentially larger than W_e. This is explained by the fact that the mean energy per relativistic electron is $\overline{\gamma} = \ln \gamma_{max} \simeq 10$, while the assumption of an equal amount of protons in the cloud immediately increases the energy by a factor of $(\Gamma - 1) m_p / m_e \overline{\gamma} \simeq 300$. An assumption that this kinetic energy has been acquired by the ejecta at initial stages of ejection, on time-scales of hours or less, would imply an acceleration power of the jet $P_{jet} \gg 10^{41}$ erg/s. Obviously, this is rather an uncomfortable requirement, but it may be significantly softened if one assumes e^+e^- pair plasma in the clouds (e.g. Liang & Li 1995; Meier 1996).

Note, however, that it is quite possible to reduce the required power in the jet down to a reasonable level even in the case of electron–proton plasma in the ejecta. Indeed, if the ejecta are continuously accelerated (and energized) on a time-scale of a day through the relativistic wind propagating in the jet region, then the power needed in the jet will be reduced to $P_{jet} \sim 10^{40}$ erg s^{-1}, which is the level of estimated kinetic power of the jets in SS 433 (e.g. Begelman et al. 1980; Margon 1984). Furthermore, if the spectrum of electrons significantly flattens below some $\gamma_1 < 100$ (for $B \sim 0.1$ G the synchrotron radiation of these electrons would be below the GHz domain), then the total number of electrons and protons may be up to 2 orders of magnitude lower than estimated above, resulting in proportional reduction of the estimated kinetic energy W_{kin} of the ejecta and the jet power P_{jet}.

2.5 Evolution of the magnetic field in time

Important information about the evolution of basic parameters in the radio clouds is found from the analysis of the observed rate of decline of the flare $S_\nu(t) \propto t^{-1.3}$ during 1994 March–April (MR94). Conclusions concerning the possible behaviour of $B(t)$ could be inferred from the condition of 'freezing' of the magnetic field lines into the highly conductive fluid. This implies that $B/\rho \propto \Delta l$, where ρ is the plasma mass density and Δl is a fluid element along the magnetic field line (see Landau & Lifshitz 1963). The plasma density depends on time as $\rho \propto M_{cl}(t)/[R(t)]^3$. Assuming now that (i) there are no strong turbulent eddies in the cloud, so the length of a fluid element in the expanding medium scales as $\Delta l(t) \propto R(t)$ and (ii) the mass of the cloud is constant, the magnetic field would be $B \propto R^{-2} \propto t^{-2}$, as long as $R \simeq v_{exp}\, t$. Then from equation (3) it follows that $S_\nu \propto N_e(t) t^{-3}$. Therefore, to account for the observed decline of radio flux, one would have to assume an increase of the total number of relativistic electrons as fast as $N_e \propto t^{1.7}$. Even neglecting adiabatic energy losses, such a behaviour of N_e implies in-situ acceleration/injection of the electrons with a rate *increasing* in time as $Q(t) \propto t^{0.7}$, and results in very rigorous requirements to be imposed on the jet energetics at the late stages. Moreover, the dependence of $B \propto R^{-2}$, which is commonly supposed in most of the previous 'expanding cloud' models (e.g. Kardashev 1962; van der Laan 1966; Band & Grindlay 1986), results in $W_B \propto R^{-1}$. Then the total energy of the magnetic field at the first stages of evolution of the cloud, e.g. when $R \leq 10^{13}$ cm (time-scales up to an hour), needs to be extremely high, $W_B > 3 \times 10^{44}$ erg, to provide $W_B \sim 3 \times 10^{42}$ erg at the stages when $R \sim 10^{15}$ cm.

These problems are overcome, if one accepts that at least one of the assumptions (i) or (ii) above does not hold. If turbulence is developed in the plasma, then in addition to stretching caused by the radial expansion of the cloud, the fluid lines will be stretched in turbulent eddies, so $\Delta l \propto R^{1+a}$ with $a > 0$, resulting in $B(R) \propto R^{-2+a}$ (a slower decline caused by the turbulent dynamo effect). If the mass of the cloud is not constant, but rather is accumulated in time as $M_{cl} \propto t^b$, then $B \propto t^{-2+b}$ (additional 'compression' effect). The magnetic field can therefore be approximated as $B \propto R^{-m} \propto t^{-m}$, and an index $m < 2$ would indicate that the magnetic fields are effectively created in and/or supplied to the clouds. Since $W_B \propto R^{3-2m}$, a power-law index $m < 1.5$ will eliminate the energetical problems for initial stages of cloud evolution. On the other hand, in the case of m significantly smaller than 1, the energy problem appears again, but now at later stages when $R \gg 10^{15}$ cm. Thus the range of $1 \leq m < 1.5$ seems most reasonable for this parameter. Then the decline $S_\nu(t) \propto t^{-1.3}$ can be explained, assuming that the total number of radio electrons in the cloud increases as $N_e \propto t^n$ with $n \simeq 1.5m - 1.3 > 0$. It is important to note that, even neglecting adiabatic and escape losses of the electrons, one needs continuous injection of radio electrons with $Q(\gamma, t) \propto t^{n-1}$, i.e. the injection may be stationary or gradually decreasing, but in any case it should be *substantial* at all stages of the flare.

2.6 The principal scenario

Summarizing this section, the following scenario for the radio flares in GRS 1915+105, or at least for the one of 1994 March 19, can be proposed. At the first stages of the outburst, the radio-emitting plasma forming a pair of radio clouds is ejected from the vicinity of the compact object, presumably a black hole, in the binary. While moving in opposite directions at relativistic speeds $\beta \simeq 0.9$, the twin clouds (with similar, but not necessarily identical, parameters) are also expanding with a high speeds, $v_{\rm exp} \sim (0.1-0.2)c$, to reach a size $R \sim (0.5-1) \times 10^{15}$ cm, and become optically transparent for synchrotron self-absorption a few days after expulsion. Relativistic electrons are continuously injected into the emission region with a spectrum $Q(\gamma, t) \sim \gamma^{-2}$ and characteristic power $P_{\rm inj} \sim 10^{38}$ erg s^{-1} or more, depending on the magnetic field $B \leq B_{\rm eq}$. These electrons may be caused by in-situ acceleration, e.g. at the bow shock front ahead of the cloud, or the relativistic wind of magnetized plasmas and/or Poynting flux propagating in the jet region (in that case, effective acceleration at the wind termination shock is plausible). An important point is that, simultaneously with injection, the electrons also escape from the cloud on energy-dependent time-scales $\tau_{\rm esc}(\gamma)$, which modifies the electron distribution $N(\gamma, t)$, and explains the steepening of the radio spectra of the fading flare from $\alpha_{\rm r} \simeq 0.5$ to $\alpha_{\rm r} \sim 1$. The decline of the flare is caused by a combination of decreasing magnetic field and decline of the injection rate $Q(\gamma, t)$, as well as adiabatic and escape losses of the radio electrons in the expanding cloud.

3 RELATIVISTIC ELECTRONS IN AN EXPANDING MEDIUM

3.1 Kinetic equation

For calculations of the synchrotron and inverse Compton fluxes expected in the framework of the scenario described above, we have to find the energy distribution function $N \equiv N(\gamma, t)$ of the electrons in these essentially non-stationary conditions. The kinetic equation describing evolution of the electrons is a well-known partial differential equation (e.g. Ginzburg & Sirovatskii 1964):

$$\frac{\partial N}{\partial t} = \frac{\partial}{\partial \gamma}(PN) - \frac{N}{\tau} + Q \, . \tag{9}$$

The Green's function solution to this equation in the case of time-independent energy losses and constant escape time $\tau(\gamma, t) =$ constant was found by Syrovatskii (1959). However, in the expanding magnetized cloud under consideration we have to suppose that *all* parameters depend on both energy γ and time t, i.e. $Q \equiv Q(\gamma, t)$ is the injection spectrum, $\tau \equiv \tau(\gamma, t)$ is characteristic escape time of a particle from the source, and $P \equiv P(\gamma, t) = -(\partial\gamma/\partial t)$ is the energy loss rate.

Strictly speaking, equation (9) corresponds to a spatially homogeneous source where the energy gain resulting from in-situ acceleration of particles is absent. Actually, however, it has much wider applications. Indeed, in a general form the equation describing evolution of the local (i.e. at the point $\boldsymbol{r}$) energy distribution function $f \equiv f(\gamma, \boldsymbol{r}, t)$ of relativistic particles can be written as (e.g. Ginzburg & Syrovatskii 1964)

$$\frac{\partial f}{\partial t} = {\rm div}(D_{\rm r}{\rm grad} f) - {\rm div}(\boldsymbol{u}_{\rm r} f) + \frac{\partial}{\partial \gamma}(P_{\rm r} f) - \frac{\partial}{\partial \gamma}(b_{\rm r} f) + \frac{\partial^2}{\partial \gamma^2}(d_{\rm r} f) \, , \tag{10}$$

where all parameters also depend on the radius vector $\boldsymbol{r}$. The first two terms on the right-hand side of this equation, where $D_{\rm r}$ is the diffusion coefficient and $\boldsymbol{u}_{\rm r}$ is the fluid velocity, describe diffusive and convective propagation of particles, the last two terms contribute to the regular and stochastic acceleration of the particles. If there are internal sources of injection and sink (such as production and annihilation) of particles, then terms similar to the last two ones in equation (9) should be added as well.

Let us consider a source where the region of effective particle acceleration can be separated from the main emission region. This seems to be the case for radio clouds in GRS 1915+105, where the probable site for in-situ acceleration of electrons may be a relatively thin region around either the bow-shock front formed ahead of the cloud or possibly the wind-termination shock formed behind the cloud, at the contact surface of relativistic wind in the jet region with the cloud. Meanwhile the main part of the observed flux should be produced in a much larger volume V_0 of the post-shock region in the cloud, since the synchrotron cooling time of radio electrons is orders of magnitude larger than the dynamical time of the source. Since acceleration efficiency (parameters $b_{\rm r}$ and $d_{\rm r}$) should significantly drop outside the shock region, after integration of equation (10) over the volume V_0 the last two terms can be neglected.

The integration of the left-hand side of equation (10) results exactly in $\partial N/\partial t$. Integration of the two propagation terms on the right-hand side of equation (10) gives the net flux of particles, resulting from diffusion and convection, across the surface of the emission region. These terms can be expressed as the difference between the total numbers of particles injected into and escaping from the volume V_0 per unit time, so the last two terms of equation (9) are found (internal sources and sinks, if present, are also implied). At last, integration of the energy loss term in equation (10) is reduced to the relevant term of equation (9), where P corresponds to the mean energy loss rate per particle of energy γ, i.e. $P = \int P_{\rm r} f {\rm d}^3 r / \int f {\rm d}^3 r$.

Thus, equation (9) is quite applicable for the study of sources with in-situ acceleration, as long as the volume V_0 where the bulk of non-thermal radiation is produced is much larger than the volume ΔV of the regions where effective acceleration of the electrons occurs. We should mention here that solutions for a large number of particular cases of the Fokker–Planck partial differential equation (including the term $\propto \bar{d}_{\rm r}$ for stochastic acceleration), corresponding to different combinations of terms responsible for time-dependent adiabatic and synchrotron energy losses, stochastic and regular acceleration, have been found earlier and qualitatively discussed by Kardashev (1962). However, only solutions for the *energy-independent* escape of relativistic particles were considered, while in our study energy dependence is a key feature for proper description of the spectral evolution of radio flares. Another important point is that the Fokker–Planck equation generally may contain

singularities, so transition from the solutions (if known) of that equation, which are mostly expressed through special functions, to the case of $\bar{d}_r \to 0$ may not always be straightforward (for a comprehensive discussion of the problems related to singularities in the Fokker–Planck equation, as well as general solutions for *time-independent* parameters, see Park & Petrosian 1995 and references therein). Meanwhile, substitution of the acceleration terms by effective injection in the regions responsible for the bulk of non-thermal radiation allows us to disentangle the problems of acceleration and emission of the electrons, and enables analytical solutions to equation (9), which are convenient both for further qualitative analysis and numerical calculations.

3.2 Time-independent energy losses

Suppose first that the escape time is given as $\tau = \tau(\gamma, t)$, but the energy losses are time-independent, $P = P(\gamma)$. The Green's function solution $G(\gamma, t, t_0)$ to equation (9) for an arbitrary injection spectrum $N_0(\gamma)$ of electrons implies δ-functional injection $Q(\gamma, t) = N_0(\gamma)\,\delta(t - t_0)$ at some instant t_0. At times $t > t_0$ it actually corresponds to the solution for the homogeneous part of equation (9), with initial condition $G(\gamma, t_0 + 0, t_0) = N_0(\gamma)$, while $G(\gamma, t_0 - 0, t_0) = 0$. Then for the function $F = PG$ this equation is reduced to the form

$$\frac{\partial F}{\partial t} = \frac{\partial F}{\partial \zeta} - \frac{F}{\tau_1(\zeta, t)}\ , \tag{11}$$

if we introduce, instead of the energy γ, a new variable

$$\zeta = g(\gamma) \equiv \int_{\gamma_*}^{\gamma} \frac{\mathrm{d}\gamma_1}{P(\gamma_1)}\,, \tag{12}$$

where γ_* is some fixed energy. Formally, ζ has the meaning of time needed for a particle with energy γ to cool down to energy γ_* (for convenience one may suppose formally $\gamma_* = 1$). The function $\tau_1(\zeta, t) = \tau[\varepsilon(\zeta), t]$, where ε is the inverse function to $g(\gamma)$ expressing the energy through ζ, i.e. $\gamma = \varepsilon(\zeta)$. The initial condition for $F(\zeta, t)$ reads

$$F(\zeta, t_0) = P[\varepsilon(\zeta)]\, N_0[\varepsilon(\zeta)] \equiv U(\zeta)\ . \tag{13}$$

Transformation of equation (11) from variables $(\zeta,\ t)$ to $(s = \zeta + t,\ u = t)$ results in a partial differential equation of only one variable for the function $F_1(s, u) = F(\zeta, t)$:

$$\frac{\partial F_1}{\partial u} = -\frac{F_1}{\tau_1(s - u, u)}\ , \tag{14}$$

with the initial condition $F_1(s, u_0) = U(s - u_0)$ found from equation (13). Integration of equation (14) is straightforward:

$$F_1(s, u) = U(s - u_0)\ \exp\left[-\int_{u_0}^{u} \frac{\mathrm{d}u_1}{\tau_1(s - u_1, u_1)}\right]\ . \tag{15}$$

In order to come back from variables $(s,\ u)$ to $(\gamma,\ t)$, it is useful to understand the meaning of the function $\varepsilon(s - x)$ that enters into equation (15) via equation (13) for U and the escape function $\tau_1 \to \tau$. Since ε is the inverse function to g, then for any z in the range of definition of this function we have $z = g[\varepsilon(z)]$. Then, taking into account that $s = \zeta + t$ and $\zeta = g(\gamma)$, for $z = s - x$ we obtain $t - x = g[\varepsilon(s - x)] - g(\gamma)$. For the function g defined by equation (12), this results in

$$t - x = \int_{\gamma}^{\Gamma_x(\gamma, t)} \frac{\mathrm{d}\gamma_1}{P(\gamma_1)}\,, \tag{16}$$

where $\Gamma_x(\gamma, t)$ corresponds to $\varepsilon(s - x)$ after its transformation to the variables (γ, t). Thus, for a particle with energy γ at an instant t, the function $\varepsilon(s - x)$ is the energy $\Gamma_x \equiv \Gamma_x(\gamma, t)$ of that particle at time x, i.e. it describes the trajectory of individual particles in the energy space.

Expressing equation (15) in terms of the Green's function $G = F/P$, the solution to equation (9) for an arbitrary $\tau(\gamma, t)$, but time-independent energy losses of particles, is found:

$$G(\gamma, t, t_0) = \frac{P(\Gamma_{t_0}) N_0(\Gamma_{t_0})}{P(\gamma)} \exp\left[-\int_{t_0}^{t} \frac{\mathrm{d}x}{\tau(\Gamma_x, x)}\right]. \tag{17}$$

Note that this is not a standard Green's function in the sense that the injection spectrum was presumed to be an arbitrary function of energy $N_0(\gamma)$, and not necessarily a delta function. Actually, it describes the evolution of relativistic particles with a given distribution $N_0(\gamma)$ at $t = t_0$. The solution for an arbitrary continuous injection spectrum is readily found after substitution of $N_0(\gamma) \to Q(\gamma, t_0)\mathrm{d}t_0$ into equation (17) and integration over $\mathrm{d}t_0$:

$$N(\gamma, t) = \frac{1}{P(\gamma)} \int_{-\infty}^{t} P(\Gamma_{t_0}) Q(\Gamma_{t_0}, t_0) \exp\left[-\int_{t_0}^{t} \frac{\mathrm{d}x}{\tau(\Gamma_x, x)}\right] \mathrm{d}t_0\ , \tag{18}$$

with the function Γ defined via equation (16). In the particular case of time- and energy-independent escape, $\tau(\gamma, t) =$ constant, this solution coincides with the one given by Syrovatskii (1959) in the form of a double integral over t_0 and Γ, if equation (18) is integrated over energy with the use of the general relations

$$\frac{\partial \Gamma_x}{\partial t} = -\frac{\partial \Gamma_x}{\partial x} = P(\Gamma_x)\ , \tag{19}$$

which follow from equation (16).

Some specific cases of equation (18) are worth brief discussion. Let the escape of particles be energy-dependent but stationary, $\tau(\gamma,t)\rightarrow\tau(\gamma)$, and consider first the evolution of $N(\gamma,t)$ when the energy losses are negligible, so $\Gamma_x\simeq\gamma$ for any t. Assuming for convenience that the form of injection spectrum does not change in time, i.e. $Q(\gamma,t)=Q_0(\gamma)q(t)$ with $q(t<0)=0$ (i.e. injection starts at t=0), equation (18) is reduced to

$$N(\gamma,t)=Q_0(\gamma)\tau(\gamma)\int_0^{t/\tau(\gamma)} q[t-\tau(\gamma)z]\,\mathrm{e}^{-z}\,\mathrm{d}z\,. \tag{20}$$

For stationary injection $q(t\geq 0)=1$ the integral results simply in $(1-\mathrm{e}^{-t/\tau})$, so $N(\gamma,t)\simeq Q_0(\gamma)\,t$ until $t<\tau(\gamma)$, and then the escape of electrons modifies the particle distribution, compared with the injection spectrum, as $N(\gamma,t)\simeq Q_0(\gamma)\,\tau(\gamma)$. In the case of $\tau(\gamma)\propto\gamma^{-\Delta}$ it results in a power-law steepening of the injection spectrum by a factor of Δ. In the case of non-stationary injection, however, the modification of $Q(\gamma)$ is different. In particular, for an impulsive injection $q(t)=\delta(t)$ it is reduced to an exponential cut-off above energies γ_t found from $\tau(\gamma_t)\simeq t$. Thus, similarly to the case of 'radiative loss break' discussed in Section 2.3, the 'escape loss break' in the energy distribution of electrons can be retained only if injection is *continuous* (but not necessarily stationary).

For a stationary injection of particles, equation (18) can be transformed to the form

$$N(\gamma,t)=\frac{1}{P(\gamma)}\int_\gamma^{\Gamma_0} Q_0(\Gamma)\exp\left[-\int_\gamma^\Gamma\frac{\mathrm{d}z}{P(z)\tau(z)}\right]\mathrm{d}\Gamma \tag{21}$$

using equation (19). In the case of $\tau\rightarrow\infty$ (absence of escape) and large t, when $\Gamma_0\equiv\Gamma_0(\gamma,t)\rightarrow\infty$, equation (21) comes to the familiar steady-state solution for a distribution of particles in an infinite medium. If the synchrotron (or IC) energy losses of electrons dominate, $P=p_2\gamma^2$, then $\Gamma_0=\gamma/(1-p_2t\gamma)$. In this case $N(\gamma,t)\sim t\,Q_0(\gamma)$ until $p_2t\gamma\leq 1$, and then the radiative losses result in a quick steepening of a *stationary* power-law injection spectrum by a factor of 1. Meanwhile, in the case of impulsive injection the modification of the initial spectrum of electrons is reduced to a sharp cut-off at $\gamma\geq 1/p_2t$.

3.3 Expanding cloud

The energy losses of relativistic electrons in an expanding medium become time-dependent. The adiabatic energy loss rate is $P_{\rm ad}=v\gamma/R$, where R is the characteristic radius of the source, and v is the speed of spherical expansion (e.g. Kardashev 1962). For the electrons of higher energies, however, the synchrotron losses may dominate. For the magnetic field we suppose $B=B_0(R_0/R)^{-m}$, where B_0 and R_0 are the magnetic field and the radius of the cloud at the instant t_0. Thus, the total energy losses can be written as

$$P=\frac{\gamma}{R}\left(p_1+p_2\frac{\gamma}{R^\mu}\right)\,, \tag{22}$$

where $\mu=2m-1$. For adiabatic losses $p_1=v$, but we do not specify parameters p_1 and p_2 to enable other losses with similar dependence on γ and R as well. Here we will suppose that expansion speed $v=$ constant, and consider evolution of the particles injected impulsively at instant t_0 with the spectrum $G(\gamma,t_0)=N_0(\gamma)$, as previously.

Since the energy losses depend on time via the radius $R(t)=R_0+v(t-t_0)$, it is convenient to pass from variable t to R. Then for the function $\Phi=\gamma G(\gamma,R)/R$, equation (9) reads

$$R\frac{\partial\Phi}{\partial R}=\gamma\frac{\partial}{\partial\gamma}\left[\left(a_1+a_2\frac{\gamma}{R^\mu}\right)\Phi\right]-\left(1+\frac{\gamma}{v\,\tau}\right)\Phi\,, \tag{23}$$

where $a_1=p_1/v$, $a_2=p_2/v$, and for τ we now imply the function $\tau(\gamma,R)$. Transformation of this equation from variables (γ,R) to $[\psi=\ln(\gamma/R^\mu),\ \xi=\ln R]$ results in the equation

$$\frac{\partial\Phi_1}{\partial\xi}=\frac{\partial}{\partial\psi}[(\mu+a_1+a_2\mathrm{e}^\psi)\Phi_1]-\left[1+\frac{\mathrm{e}^\xi}{v\,\tau_1(\psi,\xi)}\right]\Phi_1\,, \tag{24}$$

where $\Phi_1\equiv\Phi_1(\psi,\xi)$ and $\tau_1(\psi,\xi)=\tau(\mathrm{e}^{\psi+\mu\xi},e^\xi)$. The initial condition at $\xi_0=\ln R_0$ reads $\Phi(\psi,\xi_0)=R_0^{\mu-1}\mathrm{e}^\psi N_0(R_0^\mu\mathrm{e}^\psi)$. Thus, we come to an equation formally coinciding with the one considered above, with 'time' (ξ) independent 'energy' (ψ) losses $P_*(\psi)=\mu+a_1+a_2e^\psi$, and arbitrary 'escape' function $\tau_*(\psi,\xi)=(1+\mathrm{e}^\xi/v\,\tau_1)^{-1}$. The solution to this equation is analogous to equation (17):

$$\Phi_1(\psi,\xi)=R_0^{\mu-1}\,\mathrm{e}^{\Psi_0}\frac{1+c_*\mathrm{e}^{\Psi_0}}{1+c_*\mathrm{e}^\psi}N_0(R_0^\mu\mathrm{e}^{\Psi_0})\exp\left[\xi_0-\xi-\int_{\xi_0}^\xi\frac{\mathrm{e}^z\mathrm{d}z}{v\,\tau_1(\Psi_z,z)}\right]\,, \tag{25}$$

where $c_*=a_2/(\mu+a_1)$, $\Psi_0\equiv\Psi_{\xi_0}$, and $\Psi_x\equiv\Psi_x(\psi,\xi)$ is the characteristic trajectory of a particle in the 'energy' space ψ, and is readily calculated from equation (16) for the given P_*:

$$\Psi_x(\psi,\xi)=-\ln[(c_*+\mathrm{e}^{-\xi})\mathrm{e}^{(\mu+a_1)(\xi-x)}-c_*]. \tag{26}$$

Returning now to the variables γ and R, the evolution of particles with the energy distribution $N_0(\gamma)$ at the instant $R=R_0$ is found:

$$G(\gamma,R,R_0)=\left(\frac{R_0}{R}\right)^{a_1}\frac{\Gamma_{R_0}^2}{\gamma^2}N_0(\Gamma_{R_0})\exp\left[-\frac{1}{v}\int_{R_0}^R\frac{\mathrm{d}r}{\tau(\Gamma_r,r)}\right]\,. \tag{27}$$

The energy $\Gamma_r\equiv\Gamma_r(\gamma,R)$ corresponds to the trajectory of a particle with given energy γ at the instant $r=R$ in the (Γ,r) plane, and can be

represented as $\Gamma_r = \gamma\,\Lambda(\gamma, R, r)$, where

$$\Lambda(\gamma, R, r) = \frac{(R/r)^{a_1}}{1 + \frac{c_*\gamma}{R^\mu}\left[1 - (R/r)^{\mu+a_1}\right]} \cdot \tag{28}$$

In the formal case of $\mu + a_1 \to 0$, when $c_* = a_2/(\mu + a_1) \to \infty$, equation (28) tends to the limit $\Lambda' = (R/r)^{a_1}/[1 + a_2\gamma R^{a_1}\ln(R/r)]$. Note that for large γ the radiative losses may limit the trajectory of relativistic electrons at some $r_* \geq R_0$, when $\Lambda(\gamma, R, r_*) \to \infty$. For these energies Γ_{R_0} in equation (27) should be taken as ∞, but $G(\gamma, R, R_0) = 0$ as far as $N_0(\infty) = 0$.

In the general case of continuous injection of relativistic particles with the rate $Q(\gamma, t) \to Q(\gamma, R)$, the evolution of their energy distribution during expansion of the cloud between radii R_0 and $R \geq R_0$ is found, using equation (27):

$$N(\gamma, R) = G(\gamma, R, R_0) + \frac{1}{v}\int_{R_0}^{R}\left(\frac{r}{R}\right)^{a_1}\Lambda^2(\gamma, R, r)Q(\Gamma_r, r)\exp\left[-\frac{1}{v}\int_r^R \frac{\mathrm{d}z}{\tau(\Gamma_z, z)}\right]\mathrm{d}r\ . \tag{29}$$

Here $G(\gamma, R, R_0)$ given by equation (27) describes the evolution of those particles that were in the cloud by the instant R_0, while the second term describes the particles that are injected during the time interval (t_0, t). The substitution $R = R_0 + v(t - t_0)$ results in an explicit expression for $N(\gamma, t)$. If the source expands with a constant velocity v starting from $t = 0$, such a substitution results in formal changes $R \to t$, $R_0 \to t_0$, $r \to t'$ and $\mathrm{d}r = v\mathrm{d}t$ in equation (29). When only the adiabatic losses are important, i.e. $a_1 = 1$ and $a_2 = 0$, equation (28) is reduced to a simple $\Lambda = t/t_0$, and

$$N(\gamma, t) = \frac{t}{t_0}\,N_0\left(\frac{t}{t_0}\gamma\right)\exp\left(-\int_{t_0}^{t}\frac{\mathrm{d}x}{\tau(t\gamma/x, x)}\right) + \int_{t_0}^{t}\frac{t}{z}\,Q\left(\frac{t}{z}\gamma, z\right)\exp\left(-\int_z^t\frac{\mathrm{d}x}{\tau(t\gamma/x, x)}\right)\mathrm{d}z\ . \tag{30}$$

For the *energy-independent* escape, $\tau(\gamma, t) = \tau(t)$, a similar equation can be obtained from the relevant Green's function solution found by Kardashev (1962) in his case of 'stochastic acceleration + adiabatic losses + leakage' (the single combination of terms in that work where the escape term was included, but without a synchrotron loss term), if one allows the acceleration parameter to tend to zero. Another important theoretical work, where a number of solutions to the energy distribution of electrons in an expanding cloud, including both adiabatic *and* synchrotron losses, has been found, is the one by Pacini & Salvati (1973). However, their general solution is in a non-apparent form which is not easily reduced to the apparent form as given by equations (28) and (29). More importantly for our model, the escape of electrons has not been considered there at all.

It is seen from equation (30) that for a power injection $Q(\gamma) \propto \gamma^{-\alpha_{\rm inj}}$ with $\alpha_{\rm inj} > 1$ the contribution of the first term quickly decreases, so at $t \gg t_0$ only the contribution resulting from continuous injection is important. This term is easily integrated assuming stationary injection and approximating $\tau = \tau_0\gamma^{-\delta}(t/t_0)^s$, with δ and $s \geq 0$. In the case of $s < 1$, the energy distribution of electrons at $t \gg \tau(\gamma, t)$ comes to $N(\gamma, t) = Q(\gamma) \times \tau(\gamma, t)$, similar to the case of a non–expanding source. If $s \geq 1$, the condition $t \gg \tau(\gamma, t)$ can be satisfied only for large enough γ, so only at these energies can the energy-dependent escape of particles from an expanding cloud result in a steepening of $N(\gamma, t)$.

At the end of this section we remind the reader that equation (29) is derived under the assumption of a constant expansion speed v. However, it can be readily used in the numerical calculations for any profile of $v(t)$, by approximating the latter in the form of step functions with different mean speeds $\bar{v}_{\rm i}$ in the succession of intervals $(t_{\rm i}, t_{\rm i+1})$. A similar approach can also be implemented, if needed, for modelling an arbitrary profile of the magnetic field $B(R)$.

4 MODELLING OF THE MARCH 19 RADIO FLARE

In the framework of the scenario qualitatively described in Section 2, and using the results found in Section 3, in this section we study quantitatively the time evolution of the fluxes of the 1994 March 19 radio flare of GRS 1915+105 detected by Mirabel & Rodriguez (1994) and Rodriguez et al. (1995). This prominent flare is of particular interest for the following reasons:

(i) until now it has remained a unique outburst of GRS 1915+105, in which both ejecta have been clearly resolved in VLA data and the parameters of superluminal ejecta calculated (MR94);
(ii) it was a very long-lived flare observed for > 40 d;
(iii) it was a very strong outburst, with the reported accuracy of flux measurements $\simeq$5 per cent;
(iv) the time evolution of the fluxes from *both* ejecta at $\sim$10 GHz, as well as of the total fluxes at 1.4−3.3 GHz, is known.

4.1 Model parameters

For calculation of the fluxes expected in the observer frame we approximate the principal model parameters as the following functions of energy γ and time t' in the *rest frame* of a spherically expanding cloud.

(i) *Speed of expansion* is taken as

$$v_{\rm exp}(t') = \frac{v_0}{(1 + t'/t_{\rm exp})^k} \cdot \tag{31}$$

For $k > 0$ this form of $v_{\rm exp}(t')$ enables deceleration of the expansion of the cloud at times $t' \geq t_{\rm exp}$. The radius of the cloud is

$$R(t') = \frac{v_0\,t_{\rm exp}}{1 - k}\left[\left(1 + \frac{t'}{t_{\rm exp}}\right)^{1-k} - 1\right] \cdot \tag{32}$$

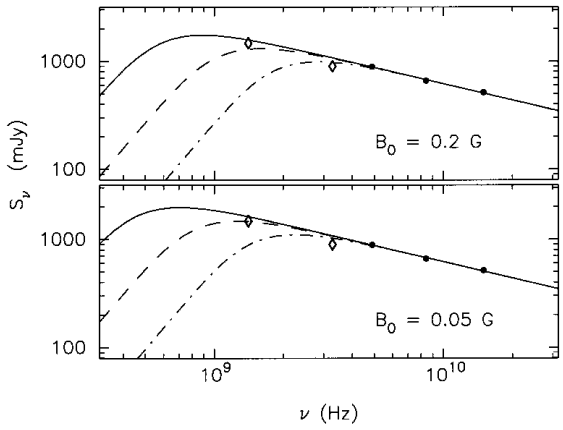

Figure 2. The spectral fluxes expected from GRS 1915+105 at $t_0 = 4.8$ d after ejection of a pair of relativistic plasmoids, $\beta = 0.92$, in the case of different magnetic fields B_0 at the instant $t = t_0$ and different expansion speeds $v_{\rm exp}(t') = v_0$. The curves shown by solid, dashed and dot–dashed lines correspond to $v_0 = 0.2c$, $0.1c$ and $0.05c$, respectively. Other model parameters in equations (32)–(38) are $m = 1$, $\alpha_{\rm inj} = 2$, $t_{\rm inj} = 20$ d ($\gg t_0'$), and $C_\lambda \to 0$. All curves are normalized to a flux of 655 mJy at $\nu = 8.42$ GHz. The fluxes measured by the Nancay and VLA radio telescopes (Rodriguez et al. 1995) on March 1994 24 are shown by diamonds and full dots, respectively. The 5 per cent error bars for the reported accuracies of these measurements are about the size of the full dots.

(ii) The mean *magnetic field* is supposed to decrease with radius R as

$$B(t') = B_0 (R/R_0)^{-m}. \tag{33}$$

Here R_0 is the cloud radius at the intrinsic time $t_0' = 2.7$ d after ejection (March 19.8). This time in the rest frame of the approaching cloud corresponds to the observer's time $t_0 = t_0'/\delta = 4.8$ d, when the flare was detected by the VLA telescope (March 24.6).

(iii) The *injection rate* of the electrons into each of the twin clouds is taken in the form of $Q(\gamma, t') = Q_0(\gamma)\, q(t')$, with

$$q(t') = (1 + t'/t_{\rm inj})^{-p}\,, \tag{34}$$

which enables the decline of injection rate at $t' \geq t_{\rm inj}$, and

$$Q_0(\gamma) \propto \gamma^{-\alpha_{\rm inj}} {\rm e}^{-\gamma/\gamma_{\rm c}}\,. \tag{35}$$

In this section we do not specify the exponential cut-off energy $\gamma_{\rm c}$, assuming only that $\gamma_{\rm c} \geq 10^4$ to account for the radio data. The coefficient of proportionality in equation (35) is chosen so as to provide the total flux of 655 mJy detected at 8.42 GHz on March 24.6 (MR94).

(iv) The *escape time* τ is approximated as follows. Let $\lambda_{\rm sc}$ be the mean scattering length of the electrons in the cloud. Then the diffusion coefficient $D \simeq \lambda_{\rm sc} c/3$, and the characteristic escape time can be estimated as $\tau \sim R^2/2D \simeq 1.5R^2/c\lambda_{\rm sc}$. If the diffusion were close to the Bohm limit, which corresponds to $\lambda_{\rm sc}$ of about the Larmor radius $r_{\rm L} = m_{\rm e}c^2\gamma/eB$ of particles, then $\tau \propto R^{2-m}\gamma$. In this case, however, the escape time of $\gamma \leq 10^3$ electrons from the radio cloud with $R_0 \sim 10^{15}$ cm and $B_0 \sim 0.1$ G would exceed 10^6 yr. Thus, in order to provide escape times of the order of a day, the diffusion of GeV electrons in the clouds should proceed many orders of magnitude faster than in the Bohm limit. Then, a more flexible approximation for $\lambda_{\rm sc}$ would be

$$\lambda_{\rm sc}/R = C_\lambda (R/R_0)^u (\gamma/\gamma_*)^\Delta\,, \tag{36}$$

with the index $u \sim 1$ being a free parameter. For the normalization energy we take $\gamma_* = 2 \times 10^3$ (i.e. $E_* = 1$ GeV). Since τ cannot be less than the time of rectilinear escape of electrons from the cloud, we come to

$$\tau(\gamma, R) = \frac{R}{c}\left[1 + \frac{3}{2C_\lambda}\left(\frac{R}{R_0}\right)^{-u}\left(\frac{\gamma}{\gamma_*}\right)^{-\Delta}\right]. \tag{37}$$

To estimate C_λ, we remember that at times of flare maximum $t' \simeq t_0$ the electron distribution $N(\gamma, t')$ in the range of $\gamma \sim 300$ should *not* be significantly modified by the escape, which requires $\tau(300, R_0) \geq t_0 \sim R_0/v_0$. Meanwhile at $t' \sim$ few times t_0 the steepening of the radio spectrum is significant (see MR94), so $\tau[300, R(3t_0)] \leq 3\, t_0$. These two requirements result in a rough estimate $C_\lambda \sim 0.1-1$. Note that since in the case of $\Delta \simeq 1$ the energy-dependent term in equation (37) quickly decreases with increasing energy, for the electrons with $\gamma \gg \gamma_*$ the escape time becomes energy-*independent*, $\tau \simeq R/c$, resulting in rather unusual spectra of relativistic electrons in the ejecta.

Thus, the principal parameters of our model are v_0, $t_{\rm exp}$ and k for the speed of expansion, B_0 and m for the magnetic field, $\alpha_{\rm inj}$, $t_{\rm inj}$ and p for the electron injection spectrum, and C_λ, u and Δ for the electron escape time. Some of these parameters, such as $\alpha_{\rm inj} \simeq 2$ or $\Delta \simeq 1$, can be limited rather tightly using the arguments discussed in Section 2. To define the range of freedom of other parameters, especially of those which describe the time evolution of the flare, detailed quantitative calculations and comparison with observed fluxes are needed.

4.1.1 Initial expansion speed and magnetic field parameters

To show the range of possible variations of v_0, in Fig. 2 we present the total fluxes expected in the observer frame at $t_0 = 4.8$ d after ejection of

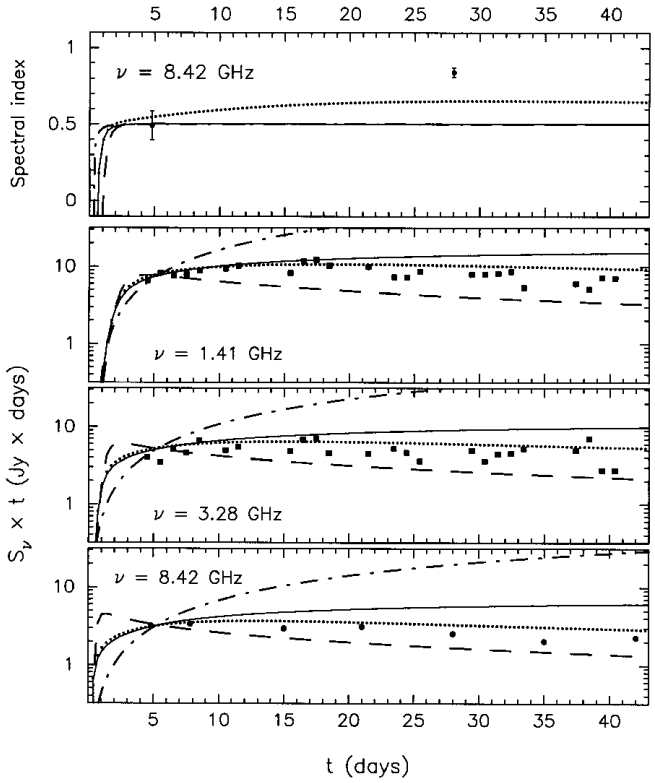

Figure 3. The temporal evolution of the fluxes at 1.41, 3.28 and 8.42 GHz, and of the spectral index at 8.42 GHz, calculated for three different values of the index m in equation (33), assuming negligible escape of electrons from the cloud, which expands with a constant speed $v_0 = 0.2c$. The curves plotted as solid, dashed and dot–dashed lines correspond to $m = 1$, $m = 1.5$ and $m = 0.5$, respectively. The dotted curves are calculated for $m = 1$ in the case of significant energy-dependent escape of the electrons, with parameters $\Delta = 1$ and $C_\lambda = 0.5$ in equation (37). Other model parameters are the same for all curves: $B_0 = 0.2$ G, $\alpha_{\rm inj} = 2$, $t_{\rm inj} = 20$ d and $p = 1$. The full squares correspond to the fluxes of the 1994 March 19 flare measured by the Nancay telescope (from Rodriguez et al. 1995), and the full dots show the fluxes of the VLA (MR94). $t = 0$ corresponds to the supposed time of ejection (March 19.8).

the radio clouds, calculated for three different expansion speeds v_0, and assuming two different magnetic fields B_0. It is seen that in the case of $B_0 = 0.2$ G, when magnetic field and relativistic electron energy densities are on the equipartition level, $w_B \simeq w_{\rm e}$, the values of $v_0 \simeq 0.1{-}0.2\,c$ can explain the observed fluxes. Assumption of $B_0 = 0.05$ G results in a better agreement of calculated and observed fluxes for $v_0 = 0.1c$ (dashed curves), but the values of $v_0 \sim 0.05\,c$ still are not acceptable. Calculations show that even for relatively weak flares, like the one reported by Gerard (1996), one has to suppose very high speeds of expansion of radio clouds, $v_0 \simeq 0.1{-}0.2c$.

Numerical calculations also confirm the estimates in Section 2 for the equipartition magnetic field $B_{\rm eq} \sim 0.2{-}0.3$ G at times $t \simeq t_0$, as well as the fast increase of the ratio $\eta = w_{\rm e}/w_B$ and the required initial injection power $P_{\rm inj} = m_{\rm e}c^2 \int \gamma\, Q_0(\gamma){\rm d}\gamma$ of relativistic electrons in the case of $B_0 < B_{\rm eq}$. For example, the fluxes corresponding to the case of $v_0 = 0.2c$ in Fig. 2 require $P_{\rm inj} = 1.2 \times 10^{38}$ erg s^{-1} (in the energy range $\gamma \leq 10^4$) if $B_0 = 0.2$ G, and $P_{\rm inj} = 10^{39}$ erg s^{-1} if $B_0 = 0.05$ G. Note that for a fixed B_0, but different values of other model parameters the values of $P_{\rm inj}$ may change, within a factor of $\sim$3, owing to different rates of adiabatic and escape losses. Thus, for the fluxes shown in Fig. 2 in the case of $B_0 = 0.2$ G, but $v_0 = 0.1\,c$, the injection power $P_{\rm inj} = 4.9 \times 10^{37}$ erg s^{-1} is needed.

In Fig. 3 we show the temporal evolution of the fluxes calculated for the clouds expanding with constant speed $v_{\rm exp}(t) = 0.2c$, assuming $B_0 = 0.2$ G but three different values of the power-law index m in equation (33). The fluxes plotted with solid, dashed and dot–dashed lines correspond to negligible escape of electrons from the clouds. One might conclude from Fig. 3 that for proper interpretation of the observed decline of $S_\nu(t)$ the index m needs to be about 1.2−1.3. However, the upper panel in Fig. 3 clearly shows that without energy-dependent escape there is no spectral steepening of the fluxes at later stages of the flare, as observed. The dotted curve in Fig. 3, calculated for $m = 1$ assuming energy-dependent escape, shows noticeable but still insufficient evolution of the spectral index $\alpha_{\rm r}$. At the same time, the decline of radio fluxes becomes faster, and now agrees well with the observed slope of $S_\nu(t)$. This allows us to conclude that, most probably, the decrease of magnetic field in the expanding cloud occurs with the power-law index $m \simeq 1$, so in further calculations we fix this parameter at $m = 1$.

Interestingly, for this value of m the ratio $\eta = w_{\rm e}/w_B$ remains at some fixed level during the expansion of the cloud, $\eta(t) \sim$ constant. Indeed, the magnetic field energy density in a cloud, expanding with some mean $\overline{v_{\rm exp}}$, is decreasing $\propto t^{-2m}$, while the time behaviour of the energy density of relativistic electrons can be roughly estimated as $w_{\rm e} \propto \overline{q}\, t/R^3 \propto t^{-2}$, so $\eta \propto t^{2(m-1)} \simeq$ constant.

4.1.2 Time profiles of the expansion, injection and escape rates

Although the dotted curve in Fig. 3 reveals noticeable steepening of the radio spectrum, it does not explain the spectral index $\alpha_{\rm r} \simeq 0.84$

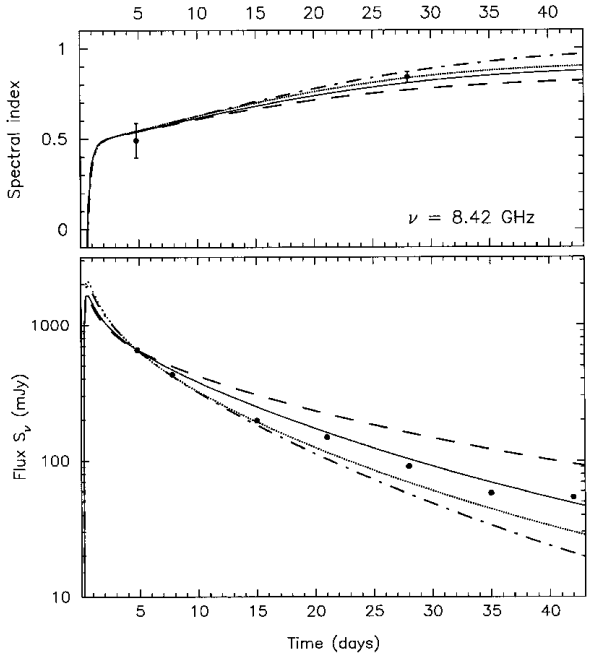

Figure 4. The evolution of the flux S_ν and spectral index α_r at 8.42 GHz expected in the cases of different relations between the expansion and injection model parameters in equations (31) and (34): $p = 2k$ and $t_{inj} = 2t_{exp}$ (solid lines), $p = k$ and $t_{inj} = t_{exp}$ (dashed lines), $p = 3k$ and $t_{inj} = 2t_{exp}$ (dot–dashed lines), $p = 2k$ and $t_{inj} = t_{exp}$ (dotted lines). For all cases $k = 0.75$ and $t_{exp} = 2$ d are supposed. Other model parameters are $\alpha_{inj} = 2$, $v_0 = 0.2c$, $B_0 = 0.3$ G, $m = 1$, $C_\lambda = 0.35$, $u = 1.5$ and $\Delta = 1$.

measured on April 16 (MR94). Our attempts to fit the observed spectra in a simple model, assuming a constant speed of expansion $v_{exp}(t') =$ constant and stationary injection rate (i.e. $t_{inj} \gg t'_0$), failed. As we have discussed in Section 3.3, for stationary injection the energy-dependent escape of relativistic electrons may result in significant steepening of $N(\gamma, t)$ only on time-scales $t > \tau(\gamma, t)$. Meanwhile, the spectral index $\alpha_r \simeq 0.5$ on March 24 implies $t < \tau(\gamma, t)$ at $t \leq t_0$ and electron energies $\gamma \leq 10^3$ (i.e. the ones responsible for the radio emission). Then, for the escape time given by equation (37), it is difficult to expect sufficiently fast increase of the ratio t/τ on time-scales of few times t_0.

Meanwhile, modification of the electron distribution $N(\gamma, t)$ because of energy-dependent escape may be more efficient (faster) if the injection rate of new electrons at times $t \geq t_0$ gradually decreases, and, simultaneously, the expansion of the clouds decelerates (that enables faster escape). This implies that both model parameters t_{exp} and t_{inj} in equations (31) and (34) are of order of t'_0. The study of possible correlations between expansion and injection rates reveals that the best fits to the observed evolution of both $S_\nu(t)$ and $\alpha_r(t)$ are reached when $t_{exp} \sim$ few days, $k \sim 0.7-1$, and, more importantly, when the time profiles of the injection rate and the speed of expansion are related as $p \simeq 2k$ and $t_{inj} \sim 1-2t_{exp}$. In Fig. 4 we show the spectra calculated for $t_{exp} = 2$ d and $k = 0.75$, assuming different combinations of the ratios t_{inj}/t_{exp} and p/k. Note that both curves corresponding to $p = 2k$ (solid and dotted lines) provide reasonable agreement with the observed slopes of both $S_\nu(t)$ and $\alpha_r(t)$.

As far as the escape rate is concerned, calculations show that, in agreement with qualitative estimates above in this section, the value of parameter C_λ in equation (37) may vary in the range $0.1-1$, so $C_\lambda \sim 0.3$ is usually taken, and the power-law index $u \simeq 1.5$.

Thus, the model parameters that enable fits of the temporal evolution of both spectral index and total flux observed during the prominent March/April radio flare of GRS 1915+105 can be fixed rather tightly as follows: $\alpha_{inj} \approx 2$, $\Delta \approx 1$, $m \approx 1$, the expansion speed $v_0 \simeq 0.1-0.3c$, depending on $B_0 \simeq 0.03-0.3$G at the time $t = t_0 = 4.8$ d (i.e. on March 24.6), the escape parameters $C_\lambda \sim 0.3$ and $u \simeq 1.5$. The characteristic expansion time $t_{exp} \sim$ a few days (in the rest frame of the cloud), injection time $t_{inj} \sim 1.5\, t_{exp}$ and $p \simeq 2k$ with $k \simeq 0.7-1$.

4.2 Injection powered by a beam in the jet region

The relation $p \simeq 2k$, with $t_{inj} \sim 1.5\, t_{exp}$, implies an interesting interpretation for the primary source of power for continuous injection/acceleration of relativistic electrons. Namely, this kind of temporal behaviour of $q(t')$ corresponds, in particular, to a scenario when the power p_{inj} of relativistic electrons injected into the cloud per unit surface area decreases with time as $p_{inj} \propto (t')^{-2}$. Then at initial stages, when the cloud expands with a constant speed $v_{exp}(t') \simeq v_0$, the injection rate $q(t') \propto R^2 p_{inj} =$ constant. At times $t' \sim t_{exp}$, when the expansion starts to decelerate, $q(t')$ also starts to decline. As follows from equation (32), at times $t' \gg t_{exp}$ the radius $R(t') \propto (t'/t_{exp})^{1-k}$ for $k < 1$, and $R(t') \propto \ln(t'/t_{exp}) \sim$ constant for $k = 1$. Therefore, in the case of $k \leq 1$, the total injection power at $t' \gg t_{exp}$ will be $q(t') \propto (t'/t_{exp})^{-2k}$, i.e. $p = 2k$ as needed. Interestingly, it is also possible to understand why t_{inj} in equation (34) is somewhat larger than t_{exp}: an expanding cloud needs some time of order of $\Delta t' \sim t_{exp}$ *after* the beginning of deceleration for a significant deviation of $R(t')$ from the linear behaviour $v_0 t'$.

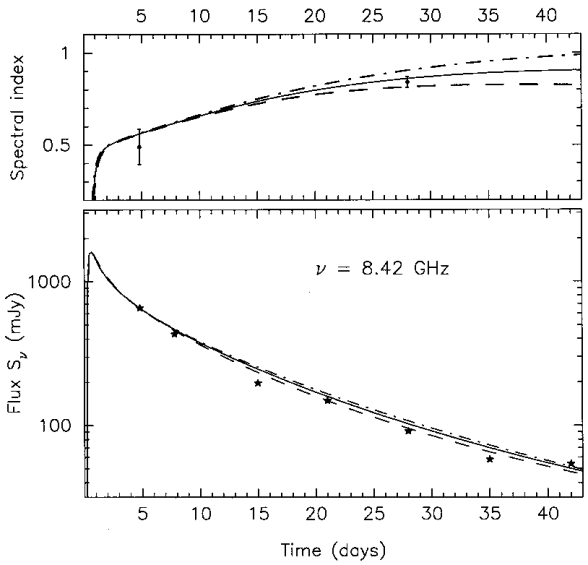

Figure 5. The evolution of the fluxes and spectral indexes at 8.42 GHz, calculated for the 'beam injection' profile of relativistic electrons, $q_b(t')$, assuming three different profiles for the expansion speed $v_{exp}(t')$, with the index $k = 1$ (solid curves), $k = 0.7$ (dashed curves) and $k = 1.3$ (dot–dashed curves). In all cases the time $t_{exp} = 2.5$ d, and the initial expansion speeds v_0 are chosen so as to provide the same radius of the clouds, $R_0 = 7.1 \times 10^{14}$ cm, at the instant $t_0 = 4.8$ d: $v_0 = 0.15c$, $0.135c$, and $0.165c$ for the solid, dashed and dot–dashed curves, respectively. The escape parameters $C_\lambda = 0.25$, $u = 1.5$ and $\Delta = 1$, and the magnetic field $B_0 = 0.1$ G are supposed.

This interpretation of the time profile of $q(t')$ suggests an injection function in the form

$$q_b(t') = R^2(t')/(v_0 t')^2 \ . \tag{38}$$

Although the discussion above was related to $k \leq 1$, the time evolution of radio fluxes observed during the 1994 March/April flare can be explained with the injection rate given by equation (38) even for values of k somewhat larger than 1. In Fig. 5 we present the fluxes calculated for the injection rate $q_b(t')$ for a fixed t_{exp}, assuming three different values of the index k in the range 0.7−1.3. The values of v_0 are chosen so that for different k the cloud radius R_0 is the same. Then in all three cases the spectral indexes α_r at the instant t_0 practically coincide.

Remarkably, the decline of the specific injection rate $p_{inj} \propto t^{-2}$ suggests a scenario where the injection of electrons is powered by a conical *beam of continuous flux of energy* from the central engine. Such a beam may be in the form of a relativistic wind of magnetized relativistic plasmas and/or electromagnetic waves (Poynting flux) propagating in the conical jet region. Then the energy flux density on the surface of a cloud departing from the central source at a constant speed would decrease $\propto t^{-2}$, as long as the total energy flux propagating in the jet is on a constant level. In this scenario the relativistic electrons may be either directly supplied by the beam, or accelerated on the *reverse shock* front terminating the wind. Here we point out that the most probable scenario for the explanation of relativistic electrons in the Crab Nebula up to 10^{15} eV implies their acceleration on the reverse shock, at a distances ∼0.1 pc, which terminates the ultrarelativistic magnetized wind of e^+e^- plasma produced by the pulsar (e.g. Kennel & Coroniti 1984; Arons 1996).

Note that in the framework of the scenario where the *bow shock* ahead of the ejecta is supposed to be responsible for in-situ acceleration of radio electrons, interpretation of the $p_{inj} \propto t^{-2}$ law is not so obvious, especially if one takes into account the fact that the ejecta detected during the March/April flare of GRS 1915+105 did not show any noticeable deceleration. Although we cannot exclude such a possibility (which would require a detailed study involving spatial profiles of the density and temperature distributions of the ambient gas), for convenience further on we will refer to equation (38) as the case of 'beam injection', and will use this injection profile, reducing the number of free model parameters.

4.3 Pair of radio clouds

So far we have considered the temporal evolution of the *total* fluxes of the 1994 March/April radio flare of GRS 1915+105. Below we discuss what kind of information can be extracted from radio data of the *resolved pair* of radio sources.

4.3.1 Flux ratio: an asymmetry between ejecta

Resolution of the pair of ejecta for the March 19 flare of GRS 1915+105 has immediately provided information of a new quality about superluminal jets. Indeed, when the pair of oppositely moving radio clouds can be resolved, then in addition to the equation for the observed angular speed μ_a of the approaching cloud, two more equations become available, namely the equation for the angular speed of the receding cloud μ_r and the equation for the ratio of the flux densities detected from two sources. The equations for μ_a and μ_r immediately allowed accurate calculations of both the speed $\beta \approx 0.92$ and angle $\theta \approx 70^\circ$ of propagation of the sources (MR94). At the same time, availability of the

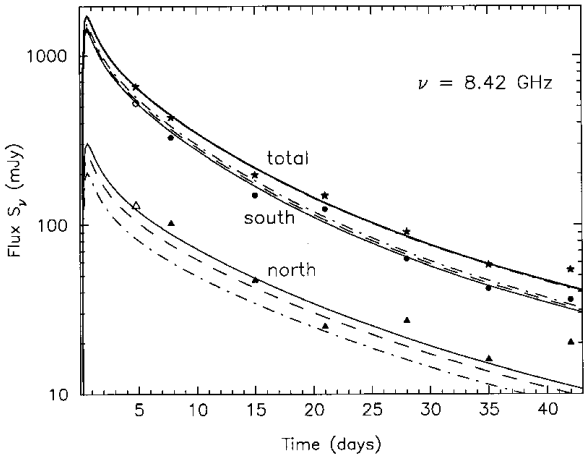

Figure 6. The fluxes expected from the approaching (*south*) and receding (*north*) radio clouds, in the case of three different flux ratios at equal intrinsic times, $S_a/S_r = 7$ (solid curves), 9 (dashed curve), and 13 (dot–dashed curve), calculated under the assumption of equal intrinsic luminosities, $L'_a = L'_r$, but allowing for the speeds of the bulk motion of the 'twin' ejecta, in these three cases equal to ($\beta_a = 0.926$, $\beta_r = 0.902$), ($\beta_a = 0.923$, $\beta_r = 0.908$) and ($\beta_a = \beta_r = 0.918$), to be different. The cloud expansion speed $v_0 = 0.14c$ and escape parameter $C_\lambda = 0.3$ are supposed. All other model parameters are equal to those in the case of $k = 0.7$ in Fig. 5. The data points plotted by stars correspond to the total fluxes, and the full dots and full triangles show the fluxes detected by Mirabel & Rodriguez (1994) from the approaching and receding components of the March 19 radio flare. The open circle and open triangle, corresponding to the fluxes of 525 mJy and 130 mJy, respectively, are plotted as demonstration of a possible sharing of the 655-mJy total flux between southern and northern components, which were not resolved on March 24 (see MR94).

flux ratio has led to significant controversy in the interpretation of the deduced value of β: is this the *true* speed of propagation of discrete *radio clouds*, or does it correspond only to some *radio patterns* moving in a spatially continuous radio-emitting fluid in the jets (Bodo & Ghisellini 1995)? Obviously, the answer to this question is of key importance for the validity of our model.

The problem is that observations of Mirabel & Rodriguez (MR94) have shown the flux ratio of the approaching to receding jets taken at equal angular separations from the core to be $(S_a/S_r)_\phi = 8 \pm 1$, while the predicted value was $(S_a/S_r)_\phi = (\mu_a/\mu_r)^{j+\alpha_r}$, where the index is $j = 3$ for the flux ratio expected from the pair of discrete radio clouds, or $j = 2$ in the case of continuous stationary jets (e.g. Lind & Blandford 1985). Then, for the observed values of $\mu_a = 17 \pm 0.4\,\mathrm{mas\,d^{-1}}$, $\mu_r = 9.0 \pm 0.1\,\mathrm{mas\,d^{-1}}$ and $\alpha_r = 0.84 \pm 0.04$ (MR94), in the case of moving radio clouds ($j = 3$) one expects the flux ratio $(S_a/S_r)_\phi = 13.1 \pm 1.7$, well beyond the observed ratio, which is formally much closer to the value of $(S_a/S_r)_\phi \sim 6$ expected in the case of $j = 2$ for a *continuous* radio-emitting jet (in disagreement with apparent picture).

A solution to this inconsistency for interpretation of the observations in terms of a real motion of radio clouds has been given in our detailed study of this problem (Atoyan & Aharonian 1997), noting that the expression $(S_a/S_r)_\phi = (\mu_a/\mu_r)^{3+\alpha_r} = [(1+\beta\cos\theta)/(1-\beta\cos\theta)]^{3+\alpha_r}$ used earlier actually implies that the jets are completely *identical*. If we suppose that the twin ejecta are *similar*, but not identical, and allow some asymmetry between them, then a more general expression for the flux ratio at equal *intrinsic times* [1] should be used:

$$\left(\frac{S_a}{S_r}\right)_{t'} \equiv \frac{S_a}{S_r} = \left(\frac{\Gamma_r}{\Gamma_a}\right)^{3+\alpha_r} \left(\frac{1+\beta_r\cos\theta_a}{1-\beta_a\cos\theta_r}\right)^{3+\alpha_r} \frac{L'_a}{L'_r}\,, \tag{39}$$

The subscripts (a, r) now distinguish between the intrinsic luminosities L', speeds β and angles of propagation θ of the approaching and receding ejecta. An asymmetry then implies at least one of the inequalities $L'_a \neq L'_r$, $\theta_a \neq \theta_r$ or $\beta_a \neq \beta_r$.

Owing to strong dependence of S_a/S_r on the ratio of Lorentz factors of the bulk motion of the clouds $\Gamma_{a,r} = 1/\sqrt{1-\beta^2_{a,r}}$ in equation (39), even the flux ratio $S_a/S_r \sim 6$ can be easily explained by a very small difference in the speeds of propagation of radio clouds. This implies that an asymmetry in the speeds of ejecta can be considered as the prime reason for the discrepancy between the measured and 'expected' flux ratios in GRS 1915+105, although some asymmetry in the intrinsic radio luminosities L'_a and L'_r, caused by a somewhat different content of relativistic electrons and/or magnetic fields in the clouds, is possible as well. Any significant difference in the angles of propagation θ_a and θ_r is less probable (at least the ejecta move in strictly opposite directions on the sky, see MR94).

In Fig. 6 we show the time evolution of the fluxes that could be expected from the approaching (*south*) and receding (*north*) radio clouds, in the case of three different flux ratios at equal intrinsic times: $S_a/S_r = 7,\ 9$ and 13. It is seen that, although the total fluxes coincide, the south-to-north partition of these fluxes is essentially different, and for the flux ratio $S_a/S_r = 7$ [for the parameters of the March 19 ejecta this corresponds to $(S_a/S_r)_\phi = 8.6$, see Atoyan & Aharonian 1997] rather good agreement of the calculated fluxes with the ones detected from both ejecta is reached. The parameters of the bulk motion of approaching and receding ejecta in that case are equal to $\beta_a = 0.926$, $\beta_r = 0.902$ and $\theta = 70.2°$, resulting in the Doppler factors $\delta_a = 0.55$ and $\delta_r = 0.33$.

[1] For asymmetrical ejecta this ratio may be slightly different from $(S_a/S_r)_\phi$.

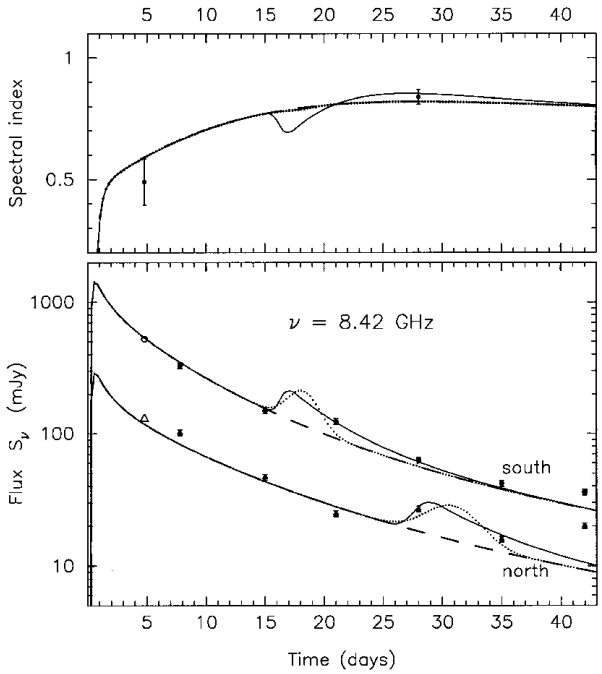

Figure 7. The temporal evolution of the fluxes (bottom panel) expected from the southern and northern radio clouds of the March 19 outburst in the case of synchronous impulsive increase of the injection rate of relativistic electrons ('electronic afterimpulse', solid lines) or of the magnetic field ('magnetic afterimpulse', dotted lines) in both plasmoids during $\Delta t \leq 1$ d around intrinsic time $t' = 9$ d after the ejection event. The top panel shows the evolution of the spectral index at 8.42 GHz expected for the *southern* component. The dashed curves correspond to the case of smooth behaviour of the electron injection and magnetic field (i.e. without any afterimpulse). The 'beam injection', with the same model parameters as in Fig. 6 (for $S_a/S_r = 7$), is supposed, except for $k = 1$ and $C_\lambda = 0.4$. The error bars on the bottom panel correspond to the 5 per cent accuracy of the measured fluxes.

4.3.2 Synchronous 'afterimpulses' far away from the core ?

It is seen from Fig. 6 that all data points for the *total* flux of the ejecta, except for the last one (on April 30), deviate from the calculated flux no more than 10 per cent, which is not too far from the reported accuracy of ~5 per cent of the fluxes measured by the VLA telescopes. The excess ~25 per cent of the total flux on April 30 can be understood if one takes into account the second ejection event, which occurred around April 23 (see MR94). Meanwhile, when we separate the fluxes measured from the *south* and *north* ejecta, the agreement becomes much worse. In particular, this relates to the fluxes of both components measured on April 9.5 (corresponding to $t = 21$ d in Fig. 6), and to the flux of receding component on April 16.5 ($t = 28$ d in Fig. 6). Changing the model parameters slightly, it is possible to reach an acceptable agreement for the flux of the receding component measured on April 16. However, the discrepancy (*excess*) ~30–40 per cent for the two other data points cannot be removed in this way, so some explanation of these fluxes is needed.

There exists a very important possibility for interpretation of these excess fluxes connected with a significant increase of the fluxes between April 4 and 5 as detected by the Nancay telescope. It is seen from table 1 in Rodriguez et al. (1995) that for 24 h between these 2 days, corresponding to $t = 16-17$ d after the ejection event, the fluxes at both 1.41 and 3.3 GHz have suddenly *increased* by ~30 per cent. The VLA was not observing GRS 1915+105 on that day, but one may suppose that the 'echo' of that suddenly enhanced radio emission (or the *secondary* flare) could be present in the flux detected by VLA from the approaching component on the next observation date, i.e. on April 9, *provided* that this secondary flare had been produced not in the central core but in the clouds [2] resolved and monitored by VLA. Then, considering the flux from the receding component, one should expect a significant *delay* between the times of observations of that event from the south and north radio clouds, if this secondary flare were due to a powerful pair of 'afterimpulses', *synchronously* sent by the central source in two opposite directions some time after main ejection on March 19.8, which would have then reached the two clouds at equal intrinsic times $t'_a = t'_r = t'$, and therefore at different apparent times $t_a = t'/\delta_a$ and $t_r = t'/\delta_r$ for approaching and receding clouds.

In Fig. 7 we show the fluxes calculated for practically the same model parameters as in Fig. 6, but assuming that there was an additional short impulse of injection of relativistic electrons into both clouds during $\Delta t' \leq 1$ d around the intrinsic time of each cloud, $t' = 9$ d after their ejection on March 19 (solid curves). For the calculated Doppler factors of counter-ejecta $\delta_a = 0.55$ and $\delta_r = 0.33$, this intrinsic time corresponds to the apparent times $t_a = 16.4$ d and $t_r = 27.2$ d for the approaching and receding clouds, respectively, i.e. between April 4 and 5 (when the increase of the unresolved flux dominated by the *approaching* component has been detected by the Nancay telescope), and April 16.0 (compared with April 16.5 when the 'excess' flux has been detected from the *receding* cloud). It is seen from Fig. 7 that the agreement of the calculated fluxes with the measured ones now becomes much better. Note that the last two data points (for April 30) in Fig. 7 cannot be

[2] We remind the reader that the ejecta have *not* been resolved by the Nancay telescope.

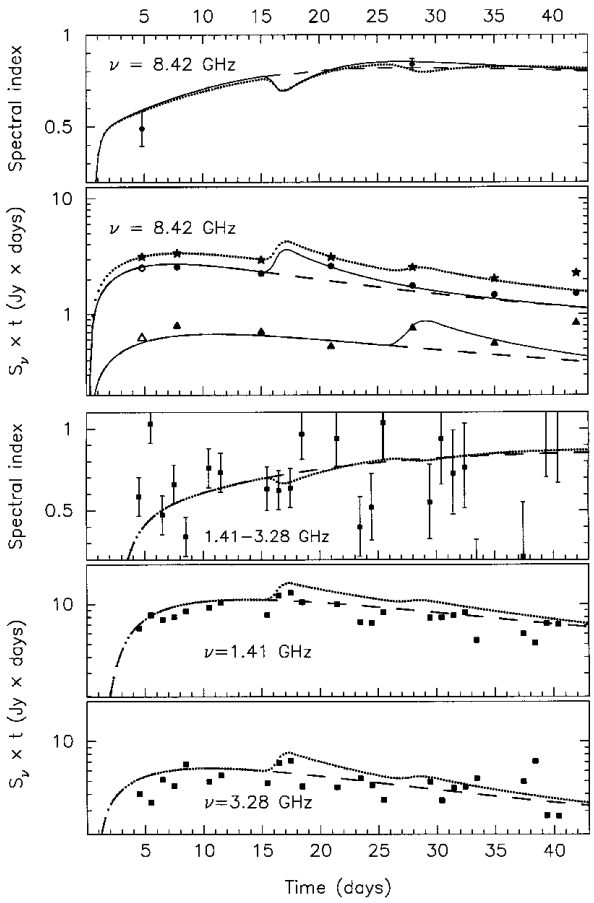

Figure 8. The same as in Fig. 7, including the Nancay data at 1.41 and 3.28 GHz (Rodriguez et al. 1995). The dotted curves in this figure show the evolution of the total fluxes and relevant spectral indexes.

explained by another afterimpulse, since they coincide in time, but rather can be connected with the second pair of plasmoids ejected around April 23 (see MR94).

If such interpretation of the data is not just an artefact, but corresponds to reality, implications for the physics of jets may be very important. It would mean that both clouds are energized by the central source even far away from it, at distances $\gg 10^{16}$ cm (!). Otherwise we have to rely upon a mere casual coincidence of intrinsic times, as well as amplitudes, of additional injection of relativistic particles from the bow shocks ahead of two counter-ejecta, which somehow would impulsively increase the rate of transformation of their kinetic energy to the accelerated electrons. Energization of the clouds from the central source implies that continuous relativistic flux of energy (*the beam*), in the form of a relativistic wind of particles and/or electromagnetic fields, should propagate in the jet region. Then the injection of relativistic electrons into the clouds could be supplied directly through this wind and/or the wind termination reverse shock on the *back* side of the clouds. The noted 'afterimpulses' could represent a pair of strong perturbations (e.g. shocks) in the continuous bidirectional flux of energy emanating from the central engine. These perturbations might remain invisible until they strike the clouds increasing electron acceleration rate.

It should be noted that in principle the excess of the radio fluxes on April 9 and April 16 from approaching and receding clouds, respectively, could also be explained by the synchronous increase of the magnetic fields in both clouds by $\sim$40 *percent* (the dotted curves in Fig. 7), without any increase in the injection rate of relativistic electrons. The principle difference between the 'magnetic' and 'electronic' afterimpulses consists of different behaviour of the spectral index α_r: if the injection of relativistic electrons proceeds smoothly, the spectral index at a given frequency also evolves smoothly, while the 'electronic' afterimpulse can result in significant hardening (variations) of the spectral index α_r. Thus, the data from multifrequency radio monitoring of the clouds will be able to distinguish between these two options.

Interestingly, some indication for temporary hardening of the radio spectra during April 4 to April 6, i.e. coincident with the time of the supposed 'afterimpulse', can be found in the data of observations of the March 19 flare at frequencies 1.41 and 3.28 GHz (see Fig. 8). Note that the agreement between calculated and measured fluxes at low frequencies is worse than at 8.4 GHz. At these frequencies, however, some allowance needs to be made for possible contribution (flickering) from the unresolved central source into the detected total flux, which may have a significant impact, in particular, on the accuracy of the deduced spectral index α_r of the clouds. One should also take into account possible effects connected with source contamination resulting from the rather high level of the background radiation at these frequencies (see Rodriguez et al. 1995).

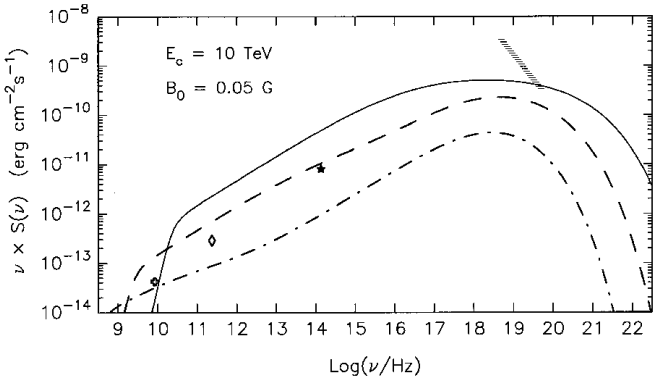

Figure 9. The spectra of synchrotron radiation that could be expected during a strong flare at three different times after ejection of radio clouds: $t = 0.1$ d (solid lines), 1 d (dashed lines) and 10 d (dot–dashed lines). Typical model parameters are supposed: $\alpha_{\rm inj} = 2$, $v_0 = 0.2c$, $t_{\rm exp} = 3$ d, $k = 1$, $\Delta = 1$, $u = 1.5$ and $C_\lambda = 0.3$. The magnetic field at the instant $t_0 = 4.8$ d is equal to $B_0 = 0.05$ G, and the exponential cut-off energy for the injected electrons is $E_{\rm c} = 10$ TeV. The cross and the diamond correspond to the level of fluxes observed during the flares of GRS 1915+105 at $\nu = 8.42$ and 234 GHz, respectively (Rodriguez et al. 1995). The star shows the flux of the IR jet observed by Sams et al. (1996), and the hatched region shows the level of the hard X-ray fluxes typically detected from the source in the energy range $\geq$20 keV during the X-ray flares (e.g. Harmon et al. 1997).

5 NON-THERMAL X-RAY AND GAMMA-RAY FLARES: PREDICTIONS

In the study of radio spectra of GRS 1915+105, in the previous sections we did not specify the maximum energies of the accelerated electrons, assuming only that the power-law distribution of the electrons injected into the expanding clouds extends to energies beyond several GeV. Meanwhile, it is not excluded that the relativistic electrons in the jets of microquasars are accelerated to much higher energies, similar to the case of jets in X-ray-selected BL Lacs, where the ultrarelativistic electrons are shown up via synchrotron X-rays and inverse Compton TeV γ-rays (e.g. Urry & Padovani 1995). Therefore, after determination from the radio data the model parameter space of the ejecta in GRS 1915+105, we consider below the fluxes of the synchrotron and IC radiations expected at higher photon frequences, provided that the spectra of electrons extend beyond TeV energies.

In that case the synchrotron radiation extends up to the X-ray/γ-ray domain. The origin of the bulk of observed X-rays in this strong X-ray transient source, with peak luminosities during the flares exceeding 10^{39} erg s^{-1} (e.g. Greiner et al. 1996), is the thermal accretion plasma around the black hole. However, since the observed X-ray spectra are rather steep, with a typical power-law index $\alpha_{\rm x} \simeq 3$ in the region of tens of keV (Harmon et al. 1997), the hard synchrotron radiation of the jets may show up at higher photon energies.

In Fig. 9 the temporal evolution of the synchrotron radiation spectra, calculated so as to provide the flux 655 mJy at $t_0 = 4.8$ d as for the March 19 outburst, are shown. Interestingly, the fluxes of high energy photons at the later stages of the flare, when the radio spectra steepen, essentially exceed the fluxes extrapolated from the radio band. This flattening is connected with an unusual shape of the electron energy distribution $N(\gamma, t)$ (see Fig. 10) which, after steepening at high energies because of energy-dependent escape $\tau(\gamma) \propto \gamma^{-1}$ given by equation (37) again flattens at very high energies, when the escape becomes energy-*independent*, $\tau \simeq R/c$.

It is seen in Fig. 9 that during the first several hours after ejection, when the cloud is still opaque at radio frequencies, the synchrotron fluxes at energies $\geq$100 keV may dominate over the extrapolation of the thermal component. This may result in a significant flattening of the overall spectrum at $E \sim 100$ keV. Although the existence of such a feature in the spectrum of GRS 1915+105 could be seen only marginally (e.g. see Sazonov et al. 1994), in the case of the second microquasar, GRO Ji655−40, the X-ray spectra clearly extend up to several hundreds of keV (see Harmon et al. 1995). Remarkably, hard tails of the X-ray spectra are a characteristic feature of other representatives of the population of galactic BH candidates as well, such as Cyg X-1 or 1E1740.7-2942 (e.g. see Grove et al. 1997). Extending this spectral feature to the

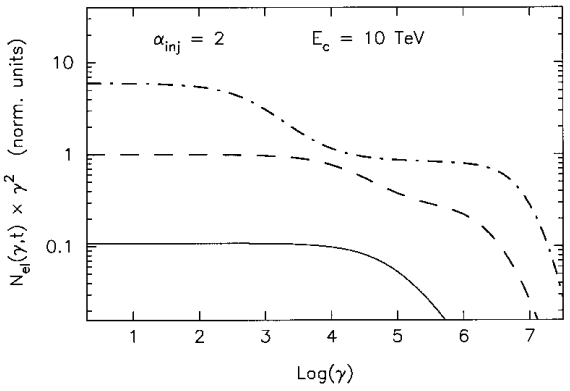

Figure 10. Temporal evolution of the energy distribution of relativistic electrons responsible for the spectra of synchrotron radiation shown in Fig. 9, and shown for the same times $t = 0.1$ d (solid lines), 1 d (dashed lines) and 10 d (dot–dashed lines).

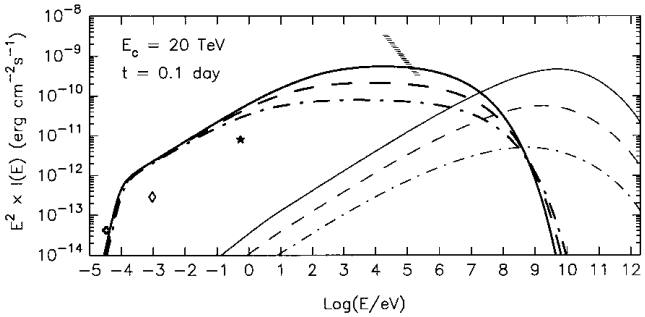

Figure 11. The fluxes of the synchrotron (heavy lines) and IC (thin lines) radiation which could be expected from GRS 1915+105 at $t = 0.1$ d after ejection of a pair of radio clouds, calculated in the case of exponential cut-off energy $E_c = 20$ TeV, assuming three different values for the magnetic field at the instant $t = t_0$: $B_0 = 0.05$ G (solid lines), 0.1 G (dashed lines) and $= 0.2$ G (dot–dashed lines). All other model parameters are the same as in Fig. 9.

extragalactic jet sources, it is worth noting that recently a variable hard X-ray spectrum well beyond 100 keV has been detected by *BeppoSAX* during the recent strong flare of the BL Lac source Mrk 501 (Pian et al. 1997).

Straightforward evidence for the acceleration of relativistic electrons beyond TeV energies in the jets of GRS 1915+105 could be provided by detection of the IC γ-rays at very high energies (VHE), $E_\gamma \geq 100$ GeV. Calculations in the the framework of the synchrotron self-Compton model show that during the strong flares one may expect detectable fluxes of VHE γ-rays, if the magnetic field in the ejected plasmoids are significantly below the equipartition level. In Fig. 11 we show the spectra of the synchrotron and IC radiation expected from GRS 1915+105 at $t = 0.1$ d after the ejection event, calculated for the same model parameters as in Fig. 9, except for somewhat higher exponential cut-off energy, $E_c = 20$ TeV, assuming three different magnetic fields B_0 at the instant t_0. It is seen that for the magnetic field $B_0 = 0.2$ G, when the ratio of the electron to magnetic energy densities, $\eta = w_e/w_B$, is at a level close to the equipartition (see Fig. 12), the fluxes of the IC γ-rays are rather small, whereas assumption of the field $B_0 \leq 0.1$ G results in a significant increase of the IC γ-rays.

Such a strong dependence of the expected IC γ-ray fluxes on the magnetic field is explained by a strong dependence of the synchrotron radiation flux on the magnetic field, $S_\nu \propto B^{1+\alpha_r}$ (e.g. Ginzburg 1979). For magnetic fields smaller by a factor of 2, one actually requires an increase of the injection rate of the electrons by a factor of 3 to provide the same radio flux. Therefore, the assumption of a different magnetic field B_0 actually corresponds to a different injection power of relativistic electrons, as shown in Fig. 12. The change of the magnetic field B_0 has an additional strong impact on the intensity of IC γ-rays, since for a given field of soft photons, the increase of the magnetic field by a factor of a results in the decrease of the ratio of the photon to magnetic field energy densities by a factor of a^2. Therefore, the share of the injection power of VHE electrons channelled into the IC γ-rays is essentially reduced.

In Fig. 13 we show the time evolution of the integral fluxes of the IC γ-rays calculated for the same parameters as in Fig. 9, but for two different energies of the exponential cut-off in the spectrum of injected electrons: $E_c = 20$ TeV (solid curves) and $E_c = 1$ TeV (dashed curves). The spectra of the hard X-rays/soft γ-rays resulting from synchrotron radiation of electrons in the case of $E_c = 20$ TeV are also shown (dot–dashed curves). The supposed magnetic field $B_0 = 0.05$ G requires the 'beam injection' power of the electrons $P_{\rm inj} \simeq 4 \times 10^{39}$ erg s^{-1}. Fig. 13 shows that in the case of acceleration of the electrons in the ejecta beyond 10 TeV, the synchrotron photons during the flare dominate up to 10 MeV over the flux of IC γ-rays. The flux of VHE γ-rays may be on the level of the Crab flux for several hours after ejection of the radio clouds. In a few days the flux drops to the level of 0.1 Crab, which is still detectable by current imaging Cerenkov telescopes in the northern hemisphere, but afterwards the source becomes invisible. It is interesting to note that during the days of very high X-ray and radio activity in 1996 May–July a marginal signal of TeV γ-rays from GRS 1915+105, with a flux at the level of $\approx$0.25 Crab, was detected by the HEGRA CT2 Cerenkov telescope (Aharonian & Heinzelmann 1998). However, this tentative result needs further confirmation by other instruments and groups.

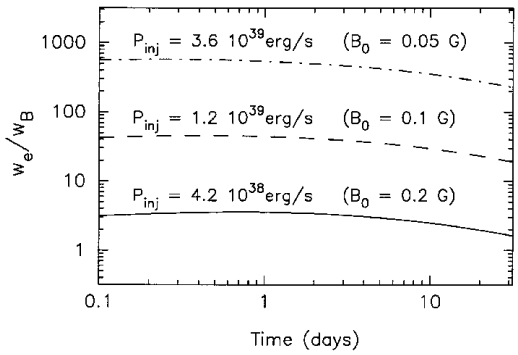

Figure 12. The ratios of the electron to the magnetic field energy densities in expanding plasmoids corresponding to the calculations in Fig. 11. Different values of the magnetic field B_0 at the instant t_0 (when the cloud radius $R = R_0 \sim 10^{15}$ cm) actually imply different injection power of relativistic electrons $P_{\rm inj}$. For the supposed $E_c = 20$ TeV, the 'equipartition' magnetic field corresponds to $B_0 \simeq 0.3$ G.

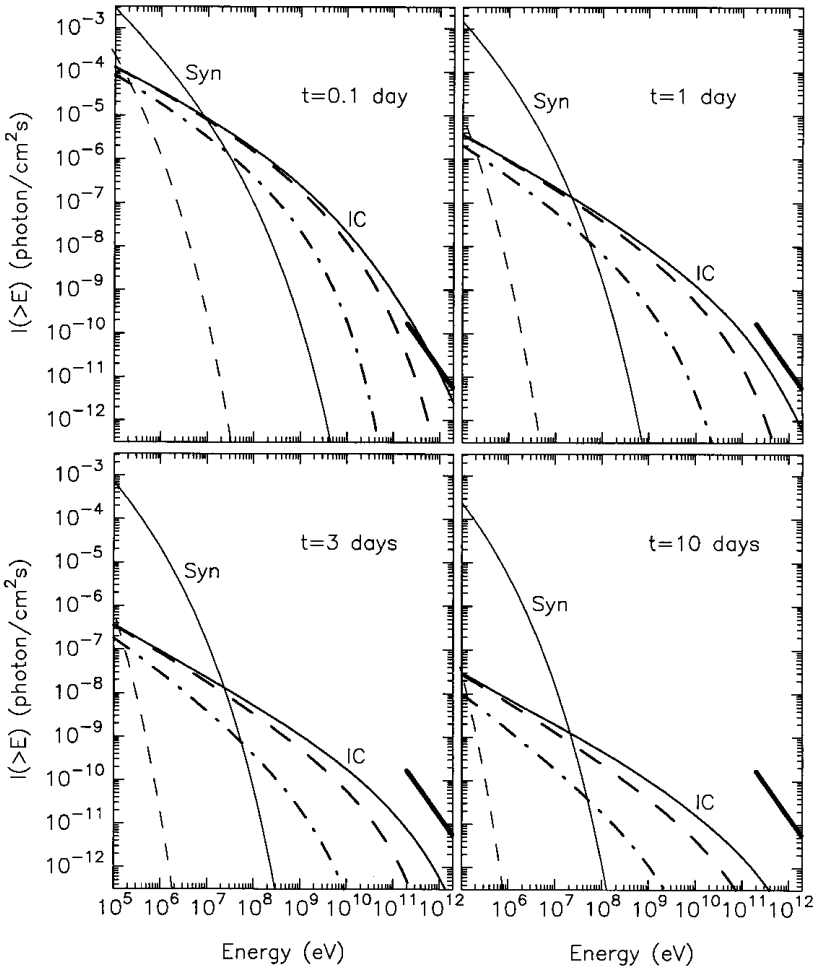

Figure 13. The fluxes of non-thermal radiation expected at different times t from GRS 1915+105 during a strong radio flare, calculated assuming three different exponential cut-off energies: $E_c = 20$ TeV (solid lines), $E_c = 1$ TeV (dashed lines) and $E_c = 30$ GeV. All other model parameters are the same as in Fig. 9. The fluxes of synchrotron and IC components are plotted by thin and heavy lines, respectively. The heavy bar shows the level of VHE flux of the Crab Nebula.

The fast drop of the flux of IC γ-rays is connected with the decrease of the total flux of the synchrotron photons, and fast expansion of the clouds, both resulting in a drastic decrease of the density of target photons. Note that the contribution caused by upscattering of the far IR radiation of the dust, which is possibly present in the vicinity of GRS 1915+105 (Mirabel et al. 1997), remains very small even if the energy density of the dust radiation is as high as that of the blackbody radiation, and the radiation temperature is small, $T \sim 100$ K, which is the most favourable condition for the IC production of the VHE γ-rays.

The fluence which could be expected at high and very high energies on different time-scales during the strong outburst is plotted in Fig. 14. For the imaging Cerenkov telescopes, with atmospheric shower collection area $\geq 10^8$ cm^2, one could expect up to hundreds of γ-rays with $E \geq 300$ GeV during a few hours of observations (one night) on the first day of the outburst. In the range of high energies, $E \geq 100$ MeV, the time-scales during which the fluxes remain on a high level do not exceed several hours. For a detector such as EGRET aboard the *Compton Gamma Ray Observatory*, with effective detection area $\sim 10^3$ cm^2, the total number of photons expected during that time does not exceed a few tens. Meanwhile, for the angular resolution of EGRET $\sim(3-5)^\circ$, the number of photons above 100 MeV from the diffuse background (Hunter et al. 1997) in the direction of GRS 1915+105 ($l = 45.37^\circ$, $b = -0.2^\circ$) during the same time is larger by a factor of 2–3. Continuation of the observations beyond the first day cannot noticeably improve the statistics of the high-energy photons, because of the strong drop of the signal at $t \geq 1$ d after ejection (see the top panel in Fig. 14). Thus, EGRET could detect such flares from GRS 1915+105, in the best case, only marginally. However, the future GLAST detector, with 2 orders of magnitude higher sensitivity because of an essentially larger effective area and better angular resolution of the photons (e.g. see Bloom 1996), will be able to detect the γ-ray flares correlated with (or slightly preceding) the radio flares from GRS 1915+105 even if the electrons in the clouds are accelerated only to the 10-GeV energy range.

6 DISCUSSION

The data of radio monitoring of the galactic microquasars, which provide a unique opportunity to follow the evolution of the fluxes from the pair of relativistic ejecta on conveniently short time-scales, contain much information on the basic parameters and processes in relativistic jets.

The temporal evolution of the radio flares in GRS 1915+105, with an apparent transition of the observed fluxes from the synchrotron

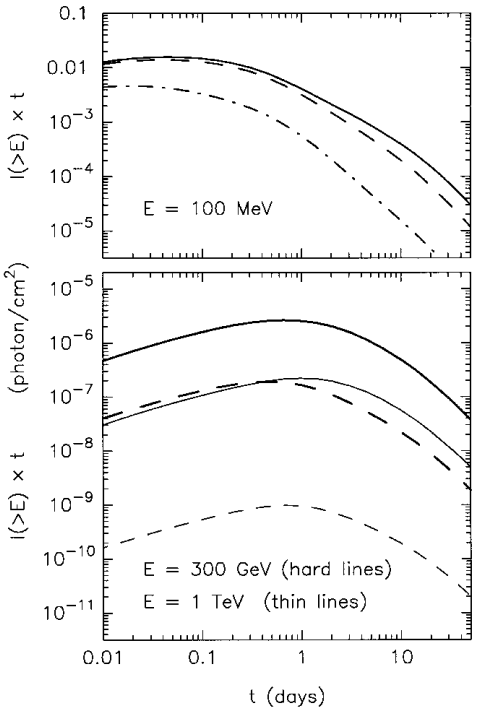

Figure 14. The fluences of the high- and very-high-energy IC γ-rays expected during strong radio flares in GRS 1915+105 in the case of three different exponential cut-off energies for the accelerated electrons: $E_c = 20$ TeV (solid curves), $E_c = 1$ TeV (dashed curves) and $E_c = 30$ GeV (dot–dashed curve). All model parameters are the same as in Fig. 13. The supposed magnetic field $B_0 = 0.05$ G implies an injection of relativistic electrons with the initial (i.e. at $t \ll t_{inj}$) power $P_{inj} \simeq (3 \pm 0.6) \times 10^{39}$ erg s^{-1}, depending on E_c.

self-absorbed to optically thin spectral forms at the fast rising stage, and later on a decline of the fluxes on time-scales of days, strongly suggests that the flares are produced in fast-expanding radio clouds ejected from the core (MR94; Rodriguez et al. 1995; Foster et al. 1996; Mirabel et al. 1998). The estimates of the characteristic parameters of the clouds show that in a few days after ejection the clouds should reach the size $R \leq 10^{15}$ cm, which implies expansion speeds $\sim(0.1-0.2)c$ in the rest frame of the ejecta. This is is in agreement with the the expansion speed deduced by Mirabel et al. (1997) from the observations of the twin radio plasmoids of the 1994 March 19 outburst, and implies extremely large broadening of the emission lines produced, if any, in the clouds, which could effectively prevent their detection in the IR band.

Estimates of the equipartition magnetic field in the clouds results in $B_{eq} \simeq 0.2-0.3$ G at the stage of maximum of radio flares. The synchrotron cooling time of GeV electrons in such magnetic fields is orders of magnitude larger than the characteristic time-scale of days during which the radio spectra often steepen from the power-law index $\alpha_r \sim 0.5$ to $\alpha_r \sim 1$. Therefore, the radiative losses could hardly be responsible for this effect, or, at least, they cannot provide a self-consistent explanation for the 1994 March/April flare (as shown in Section 2.3). We argue that for explanation of the observed steepening of radio spectra, a continuous injection of relativistic electrons into the radio clouds is needed, and propose that the prime reason for the fast modification of the energy distribution of the electrons is the energy-dependent escape of the electrons from the clouds.

In the case of magnetic fields close to the equipartition level, $B \simeq B_{eq}$, the energy $W_B + W_{el} \sim 10^{43}$ erg accumulated in the clouds in a few days after ejection is needed. This implies continuous injection of relativistic electrons with the initial power $P_{inj} \sim 10^{38}$ erg s^{-1}. However, the injection would need to be essentially more powerful, $P_{inj} \geq 10^{39}$ erg s^{-1}, if the magnetic fields were smaller than the equipartition field by a factor of 2 or more. In that case the pressure of relativistic electrons would essentially exceed the magnetic energy density in the clouds, and could then explain, at least qualitatively, fast expansion of the clouds with subrelativistic speeds $v_{exp} \geq 0.1c$.

Significant information about the processes in relativistic ejecta in GRS 1915+105 becomes available after detailed comparison of the radio data of the prominent 1994 March 19 outburst (MR94) with the results of accurate model calculations of the fluxes, produced by relativistic electrons in fast-expanding magnetized clouds. The observed rate of decline of the radio fluxes can be explained if the magnetic field declines with increasing radius of the cloud as $B \propto R^{-m}$ with $m = 1$ (see Fig. 3). This implies that the total energy of the magnetic field in the cloud is increasing as $W_B \propto R$, so it should be either effectively created in the cloud (presumably by turbulent dynamo action) or supplied from outside. Interestingly, a similar dependence of the magnetic field in the a conical jet, $B \propto r^{-1}$, but where r is the *cross-section radius* of the continuous jet (and not the cloud radius, as in our case) has been found by Ghisellini, Maraschi & Treves (1985) for BL Lac objects. Obviously, these two approximations result in the same behaviour of the magnetic field of the cloud with time, $B \propto 1/t$, as long as the cloud expands with a constant speed $v_{exp}(t) \sim v_0$, but for time-scales $t > t_{exp}$ the decline of $B(t)$ becomes different (slower).

The steepening of the radio spectra from the power-law index $\alpha_r \simeq 0.5$ on March 24 to the index $\alpha_r \simeq 0.84$ on April 16 can be explained, if both the injection of the electrons and expansion of the cloud decelerate in a few days after ejection. For interpretation of the temporal

evolution of both the spectral index and the fluxes of the March 19 outburst, the model parameters in equations (31) and (34), which describe the time profiles of the expansion speed of the clouds, $v_{\rm exp}(t')$, and of the injection rate of relativistic electrons, $q(t')$, should be connected as $t_{\rm inj} \sim (1-2)t_{\rm exp}$ and $p \sim 2k$, with $k \sim 0.7-1$ (see Fig. 4). Remarkably, these relations can be provided, if we assume that the electron injection is powered by the continuous flux of energy, in the form of a magnetized relativistic wind of particles and/or electromagnetic waves, propagating in the region of conical jet. Fig. 5 shows that the 'beam injection' profile $q_{\rm b}(t)$ can readily explain the temporal evolution of both the radio fluxes and spectral index observed at 8.42 GHz (MR94).

The data of radio monitoring of the pair of counter-ejecta in GRS 1915+105 not only allow determination of both the speed $\beta \simeq 0.92$ and angle $\theta \simeq 70^\circ$ of propagation of the ejecta (MR94), but also contain principal information of new quality, which cannot be found in the radio data when only the approaching jet is detected. Indeed, interpretation of the measured flux ratio $(S_{\rm a}/S_{\rm r})_\phi \sim 8$ of the pair of radio condensations in terms of a real motion of a pair of radio clouds implies some asymmetry between the intrinsic parameters of the jets in GRS 1915+105. Asymmetrical ejection of the pair of plasmoids would generally require, just from the momentum conservation law, a transfer of a significant *recoil* momentum to the ejection core, which is the third object in the interacting system 'two jets + core'. Comparison of this momentum with the integrated momentum (absolute values) of the gas orbiting in the inner accretion disc, which is the most probable site for production of relativistic ejecta (e.g. Blandford & Payne 1982; Begelman, Blandford & Rees 1984), suggests that asymmetrical ejection of a pair of plasmoids would be able to induce significant structural changes, or even destruction, of the inner disc, resulting in a temporary reduction/termination of the fuel supply into this region responsible for the thermal X-rays (Atoyan & Aharonian 1997).

Thus, in the framework of this scenario, the onset of subcritical/supercritical accretion would correspond to the active state of the source, with X-ray flares that can proceed both with and without powerful ejection events and, therefore, observable radio flares (Foster et al. 1996; Tavani et al. 1996). Ejection of the radio-emitting material may be accompanied by significant destruction of the inner accretion zone, which may lead to a strong decline of the X-ray fluxes *simultaneously* with production of relativistic ejecta. The time lag, up to few days, between the decline of the X-ray fluxes and appearance of strong radio flares, as observed in both superluminal microquasars GRS 1915+105 (Foster et al. 1996; Harmon et al. 1997) and GRO J1655−40 (Tingay et al. 1995; Harmon et al. 1995; Hjellming & Rupen 1995), corresponds to the time needed for expansion of the clouds to become optically transparent with respect to synchrotron self-absorption. Depending on the time needed for the recovery of the inner accretion disc after ejection, the radio flares may appear in the dips between subsequent X-ray flares (Atoyan & Aharonian 1997), as frequently observed (e.g. Harmon et al. 1997). Remarkably, this scenario is strongly supported by recent observations of Mirabel et al. (1998) of the small-scale IR−radio flares, with apparent signatures of expanding radio clouds, appearing just in the X-ray dips.

The data on the radio flux evolution of the pair of resolved ejecta contain important information on the mechanisms of continuous energization of the plasmoids. The interpretation of the ∼30 per cent excess of the fluxes detected at 8.42 GHz from the approaching and receding ejecta of GRS 1915+105 on April 9 and April 16, respectively, as the result of synchronous short-term increase (*'afterimpulse'*) of the injection rate of relativistic electrons into both clouds, as discussed in Section 4, implies continuous energization of the clouds by the central source. Then, the energy is to be supplied up to distances $\geq 3\times10^{16}$ cm by bidirectional beam, presumably in the form of a relativistic wind of particles and electromagnetic fields, emerging from the core. Note that the relations discussed above (Section 4) between parameters of the injection rate and the cloud expansion, which can be provided by the 'beam injection' profile given by equation (38), can be regarded as another indication of injection of a real beam into the clouds.

It is worth noting that the 'beam injection' scenario suggests significant softening of the hard energetical requirements rising in the framework of the conventional relativistic jet scenario that implies the kinetic energy of the bulk motion of the ejecta is the energy reservoir for in-situ acceleration of the electrons on the bow shocks formed ahead of the ejecta. Indeed, the total energy of the radio electrons injected into the clouds during first few days with the power $P_{\rm inj} \sim 10^{39}$ erg s^{-1} is about $W_{\rm inj} \sim 3\times10^{44}$ erg. If this amount of energy were from kinetic energy of the bulk motion, $W_{\rm kin}$, then the latter would be estimated as higher by at least a factor of 3 than $W_{\rm inj}$, since there was no any sign of deceleration of the bulk motion of the plasmoids beyond 1994 April (see MR94). Thus, $W_{\rm kin} \geq 10^{45}$ erg would be needed. Assuming that this amount of energy is transferred to the bulk motion 'impulsively', during a very short time-scale (since relativistic speeds imply that in hundred of seconds the ejecta will be far away from not only the inner accretion disc, but the entire binary), one has to suppose enormous power for acceleration of the ejecta, $P_{\rm jet} \geq 10^{43}$ erg s^{-1}.

Meanwhile, in the case of *continuous energy supply by the beam*, the beam power may be about $P_{\rm inj}$, which is comparable with the high luminosities observed during the X-ray flares (e.g. Greiner et al. 1996). Moreover, such a beam of relativistic energy can push the cloud forward against the ram pressure of the external medium, therefore at initial stages the plasmoids may move even with some acceleration, until they acquire enough mass and kinetic energy to continue the flight ballistically. Depending on the parameters of the external medium, the stage of significant acceleration of the ejecta could last, perhaps, up to several days, which may not be enough to see this effect in GRS 1915+105. Note that for GRO J1655−40, which is essentially closer to us, the possibility of resolving the initial acceleration could be better. Remarkably, in the beam model the acceleration of electrons may occur through the relativistic wind and/or the wind termination shock on the reverse (i.e. facing the central engine) side of the cloud , although a possible contribution from acceleration on the bow shock ahead of the cloud may not be excluded.

It is obvious, however, that this mechanism of energization of ejecta by the central engine needs further confirmation by future multiwavelength radio monitoring of another pair of powerful and long-lived radio clouds similar to the ones of the 1994 March 19 event, provided, hopefully, that GRS 1915+105 (or GRO J1655−40) will give us such an opportunity. Importantly, detection of significant

correlations between the flux variations of the twin ejecta on times scaled inversely with Doppler factors (i.e. *synchronous* in intrinsic times), could be considered as an essentially *model-independent* confirmation of the power supply from the central source, in as far as the scaling (correction) $t_a/t_r = \delta_r/\delta_a$ for the same intrinsic times depends only on the calculated Doppler factors of each ejecta.

Predictions for the fluxes expected beyond the radio domain resulting from synchrotron and inverse Compton radiation mechanisms essentially depend on the maximum energy of accelerated electrons. Assumption of the electrons accelerated beyond 10 GeV would be enough for explanation of the IR jet of GRS 1915+105 observed by Sams et al. (1996), and strongly variable IR flares of smaller scales detected by Fender et al. (1997), Mirabel et al. (1998) and Eikenberry et al. (1998). Electrons with energies $\sim$1 TeV produce synchrotron X-rays in the keV band, but even in the case of injection of relativistic electrons with $P_{\rm inj} \sim 3 \times 10^{39}$ erg s^{-1} (this corresponds to $B_0 \simeq 0.05$ G), the flux of these photons cannot exceed $\sim$10 *percent* of the thermal X-rays of the accretion disc.

However, synchrotron radiation may show up in the range of hard X-rays/soft γ-rays, if the spectrum of electrons extends to energies $\geq$10 TeV. In that case during the first several hours (up to 1 d) after the ejection event, the hard synchrotron X-ray fluxes in the range of $E \geq 100$ keV could significantly exceed the steep fluxes of thermal X-rays. In the case of $P_{\rm inj} > 10^{39}$ erg s^{-1} (i.e. if the magnetic fields in the clouds are smaller by a factor of 2-4 than the equipartition field) fluxes on the level $I(\geq 100\,{\rm keV}) > 10^{-3}$ photon/cm^{-2} s can be expected, which could be observed by the detectors like BATSE, SIGMA, OSSE or *BeppoSAX*, operating in this energy range. Meanwhile, if the magnetic and electron energy densities in the ejecta are of about equipartition level, so the injection rate of electrons is $P_{\rm inj} \sim 10^{38}$ erg s^{-1}, then the expected maximum fluxes of the synchrotron X-rays will be smaller by 1 order of magnitude. Remarkably, it be possible to detect even these fluxes with the forthcoming *INTEGRAL* mission intended for operation in the energy range 0.1$-$10 MeV. The lack of detection of variable fluxes on the level of $I(\geq 100\,{\rm keV}) \geq 10^{-4}$ photon cm^2 s during the first day after the ejection event will mean that the maximum (cut-off) energy of relativistic electrons in the ejecta is below the TeV domain.

Another, and the most straightforward, piece of evidence for TeV electrons in GRS 1915+105 could be given by detection of VHE γ-rays. Calculations in the framework of the synchrotron self-Compton model show that during strong flares one may expect detectable fluxes of TeV γ-rays, provided that the injection power of relativistic electrons $P_{\rm inj} \geq 10^{39}$ erg s^{-1} (i.e. a magnetic field in the radio clouds significantly below equipartition level). The time evolution of the IC γ-ray fluxes, shown in Figs 13 and 14, predicts that during the first few hours of a strong outburst the γ-ray fluxes above several hundred GeV are on the level of 3×10^{-11} erg/cm^{2}s, which corresponds to the level of VHE γ-ray flux of the Crab Nebula. In a few days the flux drops to the level of 0.1 Crab, which can be still detected by current imaging Cerenkov telescopes. Further on, however, the source is not detectable.

The assumption of a lower magnetic field would result in higher fluxes. However, in as far as magnetic fields significantly less than $B_0 \simeq 0.05$ G would imply an injection power of electrons $P_{\rm inj} \geq 10^{40}$ erg s^{-1}, it is difficult to expect γ-ray fluxes essentially exceeding the ones shown in Figs 13 and 14. On the other hand, in the case of in-situ acceleration/injection of electrons with $P_{\rm inj} \sim 10^{38}$ erg s^{-1} and magnetic fields on the level of equipartition, the IC fluxes decrease dramatically. Therefore either positive detection or upper limits of VHE γ-ray fluxes, being combined with hard X-ray observations above 100 keV, could provide robust constraints on the magnetic fields and efficiency of acceleration of electrons beyond TeV energies.

It is important to note, however, that owing to the narrow field of view of the Cerenkov telescopes and the opportunity of making observations only during a few night hours per day, the detection of the episodes of VHE γ-ray emission will be not an easy task. Fortunately, the predicted duration of high fluxes of VHE γ-rays is up to a few days (see Fig. 14). Then, provided that our interpretation of the observed anticorrelation/delay between strong X-ray and radio flares given above is the case, the instant of a powerful ejection event, and therefore the time (i.e. subsequent first night) most favourable for the VHE observations, can be determined, in principle, from a strong temporary drop of the thermal X-ray flux during the high state of the source. Note, however, that not necessarily all X-ray drops are connected with the ejection of plasmoids (e.g. Belloni et al. 1997; Eikenberry et al. 1998). Therefore a most reliable and timely trigger for VHE observations can be given by detections of the flares in the IR band where the clouds become transparent on very short time-scales after ejection. Importantly, the occurrence of each strong ejection event can be checked retrospectively by appearance of a strong radio flare which is 'delayed' from the time of ejection by 1–3 d.

Information about the IC γ-rays can also be obtained in the range of high energies, $E \geq 100$ MeV. It should be noted, however, that even during the first few hours of the flare, the fluxes expected in this energy range do not much exceed 10^{-6} photon cm^2 s. This implies that in the optimistic case, only marginal detection of such γ-ray flares can be expected for EGRET, which has an effective detection area $\sim 10^3$ cm^2 and angular resolution of a few degrees. We can predict, however, that the future GLAST instrument, with 2 orders of magnitude higher sensitivity than EGRET, will be able to see the γ-ray flares that would precede, by up to a few days, strong radio flares from GRS 1915+105.

ACKNOWLEDGMENTS

We express our thanks to H. J. Völk for valuable discussions. The work of AMA was supported through the Verbundforschung Astronomie/Astrophysik of the German BMBF under the grant No. 05-2HD66A(7).

REFERENCES

Aharonian F. A., Heinzelmann G., 1998, Nucl. Phys. B, 60, 193
Arons J., 1996, Space Sci. Rev., 75, 235
Atoyan A. M., Aharonian F. A., 1997, ApJ, 490, L149

Band D. L., Grindlay J. H., 1986, ApJ, 311, 595
Begelman M. C., Hatchett S. P., McKee C. F., Sarazin C. L., Arons J., 1980, ApJ, 238, 722
Begelman M. C., Blandford R. D., Rees M. J., 1984, Rev. Mod. Phys., 56, 255
Belloni T., Mendez M., King A. R., van der Klis M., van Paradijs J., 1997, ApJ, 479, L145
Blandford R. D., Payne D. G., 1982, MNRAS, 199, 883
Bloom E. D., 1996, Space Sci. Rev., 75, 109
Bloom S. D., Marscher A. P., 1996, ApJ, 461, 657
Bodo G., Ghisellini G., 1995, ApJ, 441, L69
Castro-Tirado A. J., Brandt S., Lund N., Lapshov I., Sunyaev R. A., Shlyapnikov A. A., Guziy S., Pavlenko E. P., 1994, ApJS, 92, 469
Eikenberry S. S., Matthews K., Morgan E. H., Remillard R. A., Nelson R. W., 1998, ApJ, 494, L61
Fender R. P., Pooley G. G., Brocksopp C., Newell S. J., 1997, MNRAS, 179, L65
Foster R. S., Waltman E. B., Tavani M., Harmon B. A., Zhang S. N., Paciesas W. S., Ghigo F. D., 1996, ApJ, 467, L81
Gerard E., 1996, IAU Circ. 6432
Ghisellini G., Maraschi L., Treves A., 1985, A&A, 146, 204
Ginzburg V.L., 1979, Theoretical Physics and Astrophysics. Pergamon, Oxford
Ginzburg V. L., Syrovatskii S. I., 1964, Origin of Cosmic Rays. Pergamon, London
Greiner J., Morgan E. H., Remillard R. A., 1996, ApJ, 473, L107
Grove J. E., Kroeger R. A., Skibo J. G., McNaron-Brown K., 1997, A&AS, 190, 1601
Harmon B. A., Zhang S. N., Wilson C. A., Rubin B. C., Fishman G. J., 1994, AIP Conf. Proc. 304, The Second Compton Symposium. AIP Press, New York, p. 210
Harmon B. A. et al., 1995, Nat, 374, 704
Harmon B. A., Deal K. J., Paciesas W. S., Zhang S. N., Robinson C. R., Gerard E., Rodriguez L. F., Mirabel I. F., 1997, ApJ, 477, L85
Hjellming R. M., Rupen M. P., 1995, Nat, 375, 464
Hunter S. D. et al., 1997, ApJ, 481, 205
Kardashev N. S. 1962, SvA, 6, 317
Kennel C. F., Coroniti F. V., 1984, ApJ, 283, 694
Königl A., 1981, ApJ, 234, 700
Landau L. D., Lifshitz E. M., 1963, Electrodynamics of Continuous Media. Pergamon, Oxford
Liang E., Li H., 1995, A&A, 298, L45
Lind K. R., Blandford R. D., 1985, ApJ, 295, 358
Margon B., 1984, ARA&A, 22, 507
Marscher A. P., 1980, ApJ, 235, 386
Marscher A. P., Brown R. L., 1975, ApJ, 200, 719
Meier D., 1996, ApJ, 459, 185
Mirabel I. F., Rodriguez L. F., 1994, Nat, 371, 46 (MR94)
Mirabel I. F., Rodriguez L. F., 1995, Ann. NY Acad. Sci., 759, 21
Mirabel I. F., Bandyopadhyay R., Charles P. A., Shahbaz T., Rodriguez L. F., 1997, ApJ, 477, L45
Mirabel I. F., Dhawan V., Chaty S., Rodriguez L. F., Marti J., Robinson C. R., Swank J., Geballe T., 1998, A&A, 330, L9
Pacholczyk A. G., 1970, Radio Astrophysics. Freeman, San Francisco
Pacini F., Salvati M., 1973, ApJ, 186, 249
Park B. T., Petrosian V., 1995, ApJ, 446, 699
Pian E. et al., 1997, ApJ, 492, L17
Rodriguez L. F., Gerard E., Mirabel I. F., Gomez Y., Velazquez A., 1995, ApJS, 101, 173
Sams B. J., Eckart A., Sunyaev R., 1996, Nat, 382, 47
Sazonov S. Y., Syunyaev R. A., Lapshov I. Y., Lund N., Brandt S., Castro-Tirado A., 1994, Astron. Lett., 20, 787
Shklovskii I. S., 1960, SvA, 4, 243
Syrovatskii S. I., 1959, SvA, 3, 22
Tavani M., Fruchter A., Zhang S. N., Harmon B. A., Hjellming R. N., Rupen M. P., Baylin C., Livio M., 1996, ApJ, 473, L103
Tingay S. J. et al., 1995, Nat, 374, 141
Urry M. C., Padovani P., 1995, PASP, 107, 803
van der Laan H., 1966, Nat, 211, 1131

This paper has been typeset from a T_EX/L^AT_EX file prepared by the author.